



HAL
open science

Alkaline-Earth-Catalysed Cross-Dehydrocoupling of Amines and Hydrosilanes: Reactivity Trends, Scope and Mechanism

Clément Bellini, Vincent Dorcet, Jean-François Carpentier, Sven Tobisch,
Yann Sarazin

► **To cite this version:**

Clément Bellini, Vincent Dorcet, Jean-François Carpentier, Sven Tobisch, Yann Sarazin. Alkaline-Earth-Catalysed Cross-Dehydrocoupling of Amines and Hydrosilanes: Reactivity Trends, Scope and Mechanism. *Chemistry - A European Journal*, 2016, 22 (13), pp.4564 - 4583. 10.1002/chem.201504316 . hal-01274113

HAL Id: hal-01274113

<https://univ-rennes.hal.science/hal-01274113v1>

Submitted on 3 Nov 2023

HAL is a multi-disciplinary open access archive for the deposit and dissemination of scientific research documents, whether they are published or not. The documents may come from teaching and research institutions in France or abroad, or from public or private research centers.

L'archive ouverte pluridisciplinaire **HAL**, est destinée au dépôt et à la diffusion de documents scientifiques de niveau recherche, publiés ou non, émanant des établissements d'enseignement et de recherche français ou étrangers, des laboratoires publics ou privés.

**Alkaline-earth catalysed cross-dehydrocoupling of amines and hydrosilanes:
Reactivity trends, scope and mechanism**

Clément Bellini,^[a] Vincent Dorcet,^[b] Jean-François Carpentier,^{*[a]}

Sven Tobisch,^{*[c]} and Yann Sarazin^{*[a]}

^[a] *Organometallics: Materials and Catalysis Department, Institut des Sciences Chimiques de Rennes, UMR 6226 CNRS – Université de Rennes 1, Campus de Beaulieu, F-35042 Rennes (France)*

E-mail: jean-francois.carpentier@univ-rennes1.fr; yann.sarazin@univ-rennes1.fr

^[b] *Centre de Diffractométrie des Rayons X, Institut des Sciences Chimiques de Rennes, UMR 6226 CNRS - Université de Rennes 1, F-35042, Rennes (France)*

^[c] *University of St Andrews, School of Chemistry, Purdie Building, North Haugh, St Andrews, KY16 9ST, UK*

E-mail: st40@st-andrews.ac.uk

Keywords: alkaline earths • barium • hydrosilane-amine cross-dehydrocoupling • DFT computations • mechanisms

Abstract

Alkaline-earth (Ae = Ca, Sr, Ba) complexes are shown to catalyse the chemoselective cross-dehydrocoupling (CDC) of amines and hydrosilanes. Key trends have been delineated in the benchmark couplings of Ph₃SiH with pyrrolidine or *t*BuNH₂. Ae[E(SiMe₃)₂]₂•(THF)_x (E = N, CH; *x* = 2-3) are more efficient than {N[^]N}Ae[E(SiMe₃)₂]₂•(THF)_n (*n* = 1-2) complexes bearing an iminoanilide ligand, and alkyl precatalysts are better than amido ones. Turnover frequencies (TOF) increase with Ca<Sr<Ba. Ba[CH(SiMe₃)₂]₂•(THF)₃ displays the best performance (TOF up to 3600 h⁻¹). Substrate scope (> 30 products) include di(amine)s and di(hydrosilane)s. Kinetic analysis of the Ba-promoted CDC of pyrrolidine and Ph₃SiH show that (i) the kinetic law is $rate = k [Ba]^1 [amine]^0 [hydrosilane]^1$, (ii) electron-withdrawing *p*-substituents in arylhydrosilanes improve reaction rates, (iii) a maximal kinetic isotopic effect ($k_{SiH}/k_{SiD} = 4.7$) is seen for Ph₃SiX (X = H, D). DFT computations have identified the prevailing mechanism. Instead of an inaccessible σ-bond breaking metathesis pathway, DFT provides evidence that the CDC follows a stepwise reaction path with N–Si bond-forming nucleophilic attack of the catalytically competent Ba pyrrolide onto the incoming silane, followed by rate-limiting H-transfer to Ba. The participation of Ba silyl species is prevented energetically. The trend Ca<Sr<Ba results from greater accessibility of the metal centre and increasing Ae–N_{amide} bond strength upon going down in group 2.

Introduction

The catalysis of cross-dehydrocoupling (\equiv CDC) reactions between E–H and E'–H moieties leading to the formation of E–E' bonds and release of dihydrogen as by-product, where E and E' are respectively electronegative (N, O, P) and more electropositive (B, Si) *p*-block elements, is attracting growing interest in main group chemistry.^[1] The resulting molecular or macromolecular species are useful as emissive materials, high-performance elastomers, synthetic precursors for ceramic thin films and monoliths, and in biomedicine.^[2]

Of interest to our research program, the formation of N–Si bonds yields silazanes. These are valuable as ligands in coordination chemistry,^[3] as bases,^[4] silylating agents^[5] or protecting groups for amines, indoles and anilines in organic synthesis.^[6] In addition, some oligo- and polysilazanes make for excellent precursors of Si₃N₄ ceramics.^[7] Traditional processes for the production of silazanes require metalation of amines with alkali bases or aminolysis of chlorosilanes,^[7^a,8] but these procedures involving the formation of stoichiometric amounts of salts or HCl by-products are not optimal. The impetus is now shifting towards cost- and atom-efficient methods such as the expedient catalysed N–H/H–Si cross-dehydrocoupling of hydrosilanes with HNR¹R² amines (R¹, R² = H, alkyl, aryl). Middle and late transition metal compounds where the low-valent metal centre can undergo oxidative addition, *e.g.* palladium Al₂O₃-supported species and graphene-supported nanoparticles,^[9] Ru₃(CO)₁₂ and Rh₆(CO)₁₆ clusters,^[10] or discrete ruthenium(II),^[6^b,6^e] rhodium(I),^[6^c,11] or chromium(0)^[12] complexes, first dominated the arena; a copper(I) system was also described.^[13] Notable results were later achieved with hard, oxophilic metal ions for which σ -bond metathesis or Si-to-metal hydride transfer are prominent mechanistic features. Hence, some success was met in the 1990's with Cp₂TiMe₂,^[14] while more recently Al³⁺,^[15] Y³⁺,^[16] Yb²⁺,^[17] U⁴⁺,^[18] Zn²⁺,^[19] and especially Ae²⁺ (Ae = alkaline-earth)^[17^c,20] catalysts have shown great promise. B(C₆F₅)₃ is useful for the coupling of hydrosilanes with aromatic amines.^[6^f]

Of these, alkaline-earth catalysts are particularly efficient, achieving high selectivity in the coupling of hydrosilanes and amines, hydrazines or ammonia. Harder's Ca-azametallacyclopropane $\text{Ca}(\eta^2\text{-Ph}_2\text{CNPh})(\text{HMPA})_3$ couples aliphatic amines or aniline with Ph_3SiH with a metal loading of 3–10 mol-% at 20 °C in 0.5–24 h.^[17c] Sadow's $\{\text{To}^{\text{M}}\}\text{Mg}(\text{N}(\text{SiMe}_3)_2)$ (To^{M} = tris(oxazolinyl)-borato) couples primary amines, ammonia or hydrazine with phenyl-substituted hydrosilanes.^[20a] The kinetic rate law is first-order in [silane] and [precatalyst], and zeroth-order in [amine]; mechanistic investigations suggested that the reaction proceeds by a turnover limiting nucleophilic attack of the magnesium-amide onto the silane followed by rapid hydride transfer from the hypervalent Si to the Mg centre. Hill reported that the homoleptic amido precatalysts $\text{Ae}\{\text{N}(\text{SiMe}_3)_2\}_2$ ($\text{Ae} = \text{Mg, Ca, Sr}$) operate CDC of hydrosilanes and aliphatic amines or bulky anilines at 20–60 °C (metal loading 5–10 mol-%);^[20b] no data was provided for their barium congener. The Ca precatalyst performed substantially better than its Mg and Sr analogues, as exemplified in the coupling of Et_2NH with Ph_2SiH_2 . However, several subtleties associated to the bond polarity and to charge density of the Ae ion became apparent upon mechanistic investigations. The kinetic rate law was first-order in [metal] and [amine] and zeroth-order in [silane] for Mg and Ca precatalysts, but it was second-order in [metal] and first-order in [amine] and [silane] with Sr. In a recent communication, we reported that highly active and selective Ba complexes surpass their Ca and Sr analogues for chemoselective N–H/H–Si CDC reactions;^[20c] the main mechanistic features were delineated upon combination of experiment and DFT computations. The full scope of this Ae-catalysed reaction is presented here together with a thorough DFT analysis of rival mechanistic pathways. A complete set of synthetic and catalytic data, highlighting the differences between Ca, Sr and Ba ($r_{\text{ionic}} = 1.00, 1.18$ and 1.35 Å, respectively), is provided.

Results and Discussion

Precatalyst synthesis

A broad range of Ae precatalysts, some devoid of bulky ancillary ligands and some instead stabilised by the bidentate iminoanilide $\{N^{\wedge}N\}^{-}$ ($\equiv [ArN(o-C_6H_4)C(H)=NAr]^{-}$ with Ar = 2,6-*i*Pr-C₆H₃) were initially screened in the CDC of amines and hydrosilanes (families of complexes 1–8, Figure 1). Most were prepared according to known literature protocols. The silanido compounds Ae(SiPh₃)₂•(THF)₃ (Ae = Sr, **5-Sr**; Ba, **5-Ba**) and the heteroleptic complex $\{N^{\wedge}N\}Ba\{N(SiMe_2H)_2\}•(THF)_2$ (**7-Ba**) were synthesised here for the first time. The pyrrolido complexes $\{N^{\wedge}N\}Sr\{N(CH_2)_4\}•(HN(CH_2)_4)$ (**9-Sr**), where some degree of stabilisation is ensured by a coordinated molecule of pyrrolidine ($\equiv HN(CH_2)_4$),^[21] and $\{N^{\wedge}N\}Ba\{N(SiMe_3)_2\}•(HN(CH_2)_4)_2$ (**10-Ba**) were also prepared for mechanistic purposes.

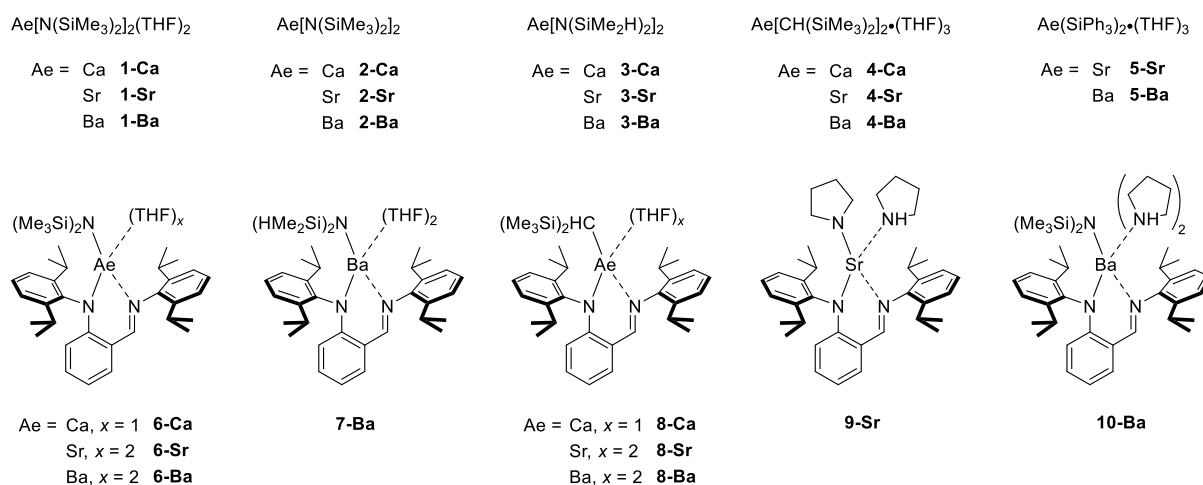


Figure 1. Ae precatalysts screened for N–H/H–Si cross-dehydrocoupling reactions.

The yellow **5-Sr** ($\delta_{29Si} = -12.14$ ppm) and the orange **5-Ba** ($\delta_{29Si} = -12.11$ ppm) were obtained in 32% and 86% in non-optimised yield, respectively, upon salt metathesis between the alkaline-earth iodides AeI₂ and 2 equiv of freshly prepared KSiPh₃^[22] in THF.^[23] The orange **7-Ba** supported by the bulky bidentate iminoanilide $\{N^{\wedge}N\}^{-}$ was synthesised by salt

metathesis of $\{N^{\wedge}N\}H$, anhydrous BaI_2 and 2 equiv of $KN(SiMe_2H)_2$ ^[24] following a known one-pot protocol.^[25] The orange strontium-pyrrolide **9-Sr** was prepared in pentane upon aminolysis of the alkyl complex **8-Sr** with excess pyrrolidine (3 equiv); on the other hand, treatment of **6-Ba** with 2 equiv of pyrrolidine merely afforded the bis-adduct **10-Ba** by displacement of THF, with no evidence for the release of $HN(SiMe_3)_2$ and formation of a Ba-pyrrolide.^[26] Diagnostic resonances in its 1H NMR spectrum include broad overlapping multiplets at δ 2.49 and at 1.27 ppm, integrating each for 8H and belonging to the coordinated pyrrolidine molecule and pyrrolide, and a broad singlet at δ 0.94 ppm for the two $HN_{pyrrolidine}$ acidic hydrogens.^[21] The presence of $N(SiMe_2H)^-$ moieties in **7-Ba** compared to the more traditional $N(SiMe_3)_2^-$ amido group in **6-Ba** is known to impart greater stability and kinetic inertness to complexes of the large alkaline-earth metals owing to the formation of intramolecular $Ba \cdots H-Si$ β -agostic interactions, although this may at times come at the expense of catalytic efficacy.^[24,27] The agostic contact in **7-Ba** is detected spectroscopically: the $^1J_{H-Si}$ coupling constant of 160 Hz in the 1H NMR spectrum and the stretching frequency ν_{Si-H} of 2004 cm^{-1} in the FTIR spectrum of the complex both testify to the existence of agostic bonding of mild intensity. Agostic distortions are better visualised in the molecular solid-state structure of the complex determined by single-crystal X-ray diffraction (Figure 2). A large discrepancy is noted between the $Ba2-N53-Si3$ ($129.7(2)^\circ$) and $Ba2-N53-Si4$ ($105.31(19)^\circ$) angles. Moreover, the four atoms $Ba2$, $N53$, $Si4$ and $H4$ (with the $Si4-H4$ bond pointing towards the metal) are nearly perfectly coplanar whereas $Ba2$, $N53$, $Si3$ and $H3$ are not. Both observations imply the presence of a single, mild $Ba2 \cdots H4-Si4$ agostic interaction,^[24-25,27-28] resulting in a formerly 6-coordinate $Ba2$ atom. By comparison, the two $Ba-N-Si$ angles ($114.85(15)^\circ$ and $119.78(14)^\circ$) in $\{N^{\wedge}N\}Ba\{N(SiMe_3)_2\} \cdot (THF)_2$ (**6-Ba**) do not show as great a difference as in **7-Ba**, and the $Ba-N_{amide}$ bond length in **6-Ba** ($2.623(3)\text{ \AA}$) is elongated *vis-à-vis* that in **7-Ba** ($2.601(4)\text{ \AA}$).^[29]

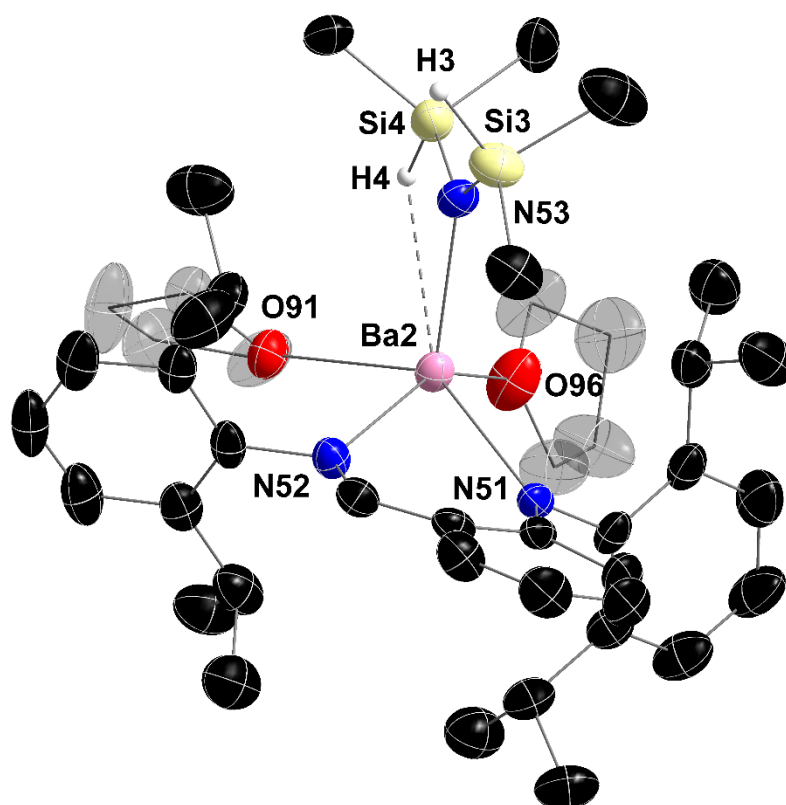
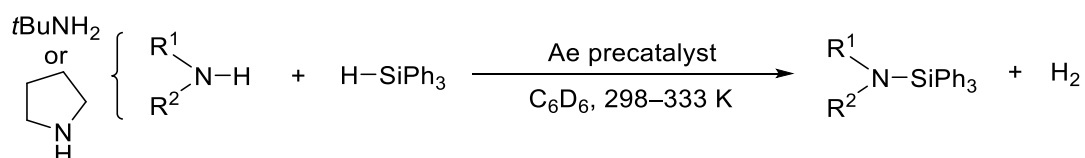


Figure 2. ORTEP representation (ellipsoids at the 50% level of probability) of the molecular solid-state structure of $\{N^N\}Ba\{N(SiMe_2H)_2\} \cdot (THF)_2$ (**7-Ba**). Only one of the two independent but geometrically equivalent molecules found in the asymmetric unit, with the main component of the disordered THF molecule corresponding to O96, is depicted. Hydrogen atoms on carbon atoms are omitted and the carbon atoms of the coordinated THF molecules are represented in shaded tone for clarity. Selected bond lengths (\AA) and angles ($^\circ$): Ba2–N53 = 2.601(4), Ba2–N51 = 2.676(4), Ba2–N52 = 2.764(4), Ba2–O96 = 2.774(3), Ba2–O91 = 2.811(3); Si4–N53–Ba2 = 105.31(19), Si3–N53–Ba2 = 129.7(2).

Precatalyst screening

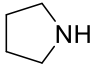
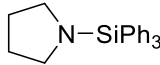
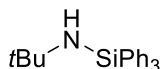
The performances of the families of complexes **1-9** as precatalysts in N–H/H–Si CDC reactions were first assessed in two benchmark reactions: the coupling of triphenylsilane with the highly reactive pyrrolidine or with the more reluctant *tert*-butylamine (Scheme 1).



Scheme 1. Benchmark cross-dehydrocoupling (CDC) reactions for initial Ae precatalyst screening.

From the results of this preliminary screening collated in Table 1, the following main lines emerge: (i) independently of the identity of the ligands, the catalytic activity increases systematically according to $\text{Ca} < \text{Sr} < \text{Ba}$ (compare the following sets of experiments: entries 9, 10 and 11, entries 15, 16 and 18, entries 20, 21 and 22, or entries 24, 25 and 26);^[30] the barium precatalysts afforded unmatched overall turnover frequency (TOF) values calculated at 75–99% conversions up to $3600 \text{ mol}_{\text{substrate}} \cdot \text{mol}_{\text{Ba}}^{-1} \cdot \text{h}^{-1}$ as in entry 13; (ii) the simple bis-amido complexes **1** are more effective than their direct heteroleptic counterparts **6** (compare entries 9 and 15, 10 and 16, or 11 and 17), the same being true of the bis-alkyls **4** and their heteroleptic derivatives **8** (compare entries 14 and 19 or 22 and 26); (iii) the presence of coordinated THF molecules in bis-amido precatalysts bears no influence on the overall catalytic efficiency (compare entries 3 and 4, or 10 and 12); (iv) the alkyl complexes are significantly more effective than their amido analogues (compare entries 1 and 2, 11 and 13 or 23 and 26); (v) the complexes incorporating $\text{N}(\text{SiMe}_2\text{H})^-$ amide afford very little, if any, catalytic activity (entries 5 and 7); (vi) the bis-silanido complex **5-Sr** (entry 6) is inactive whereas the pyrrolido compound **9-Sr** does promote catalysis competently (entry 8),^[31] two observations heavy of implications regarding the nature of the operative mechanism (*vide infra*); and (vii) even in the presence of 2 equiv of Ph_3SiH *per* amine, the very mildly reactive *t*BuNH₂ solely affords the monocoupled product *t*BuNHSiPh₃ with 100% chemoselectivity with no detectable formation of the decoupled *t*BuN(SiPh₃)₂ (entries 20–26), hence highlighting the difficulty in making RN(SiPh₃)₂ disilazanes from primary amines with this procedure.

Table 1. Alkaline-earth catalysed cross-dehydrocoupling of amines and triphenylsilane^[a]

Entry	R ¹ R ² N-H	Product	Precat.	N/Si/Ae	T ^{re} [K]	T [min]	Conv. [%] ^[b]	TOF [h ⁻¹] ^[c]
1			1-Ca	20:20:1	298	2×60	29	3
2			4-Ca	20:20:1	298	2×60	74	7
3			1-Ba	20:20:1	298	2×60	91	9
4			2-Ba	20:20:1	298	2×60	87	9
5			3-Ba	20:20:1	298	2×60	3	<1
6			5-Sr	20:20:1	298	2×60	0	0
7			7-Ba	20:20:1	298	2×60	11	<1
8			9-Sr	20:20:1	298	2×60	92	9
9			1-Ca	400:400:1	298	15×60	72	19
10			1-Sr	400:400:1	298	15×60	99	26
11			1-Ba	400:400:1	298	15	99	1584
12			2-Sr	400:400:1	298	15×60	99	26
13			4-Ba	400:400:1	298	5	75	3600
14			4-Ba	400:400:1	298	15	99	1584
15			6-Ca	400:400:1	298	15×60	42	11
16			6-Sr	400:400:1	298	15×60	74	20
17			6-Ba	400:400:1	298	15	32	512
18			6-Ba	400:400:1	298	15×60	99	26
19			8-Ba	400:400:1	298	15	63	1008
20	<i>t</i> Bu-NH ₂		8-Ca	20:20:1	333	2×60	0	0
21			8-Sr	20:20:1	333	2×60	5	<1
22			8-Ba	20:20:1	333	2×60	25	3
23			1-Ba	20:20:1	333	2×60	50	5
24			4-Ca	20:20:1	333	2×60	9	1
25			4-Sr	20:20:1	333	2×60	82	8
26			4-Ba	20:20:1	333	2×60	95	10

[a] Reactions in C₆D₆ (0.5 mL), with [Ae]₀ = 10.0 mM and [amine] = 0.2 M for [amine]₀/[Ph₃SiH]₀/[precat.]₀ = 20:20:1 or 20:40:1, and [amine] = 4.0 M for [amine]₀/[Ph₃SiH]₀/[precat.]₀ = 400:400:1; reactions times not optimised. In the case of *t*BuNH₂, entries 19-25, the formation of *t*BuN(SiPh₃)₂ was never detected. [b] Conversion of the starting amine determined by ¹H NMR spectroscopy. [c] Overall turnover frequency calculated at maximal conversion.

From the foregoing, the bis-alkyl barium complex $\text{Ba}[\text{CH}(\text{SiMe}_3)_2]_2 \cdot (\text{THF})_3$ (**4-Ba**) is evidently the precatalyst of choice for this catalysis. It is reasonably easy to prepare on a multi-gram scale compared to its more intricate heteroleptic derivative **8-Ba**. Its more robust THF-coordinated amido analogue **1-Ba**, which is admittedly easier to synthesise, also exhibit impressive performances and therefore constitutes an excellent alternative. For these reasons, in terms of substrate scope, the focus will be on these two precatalysts in the followings.

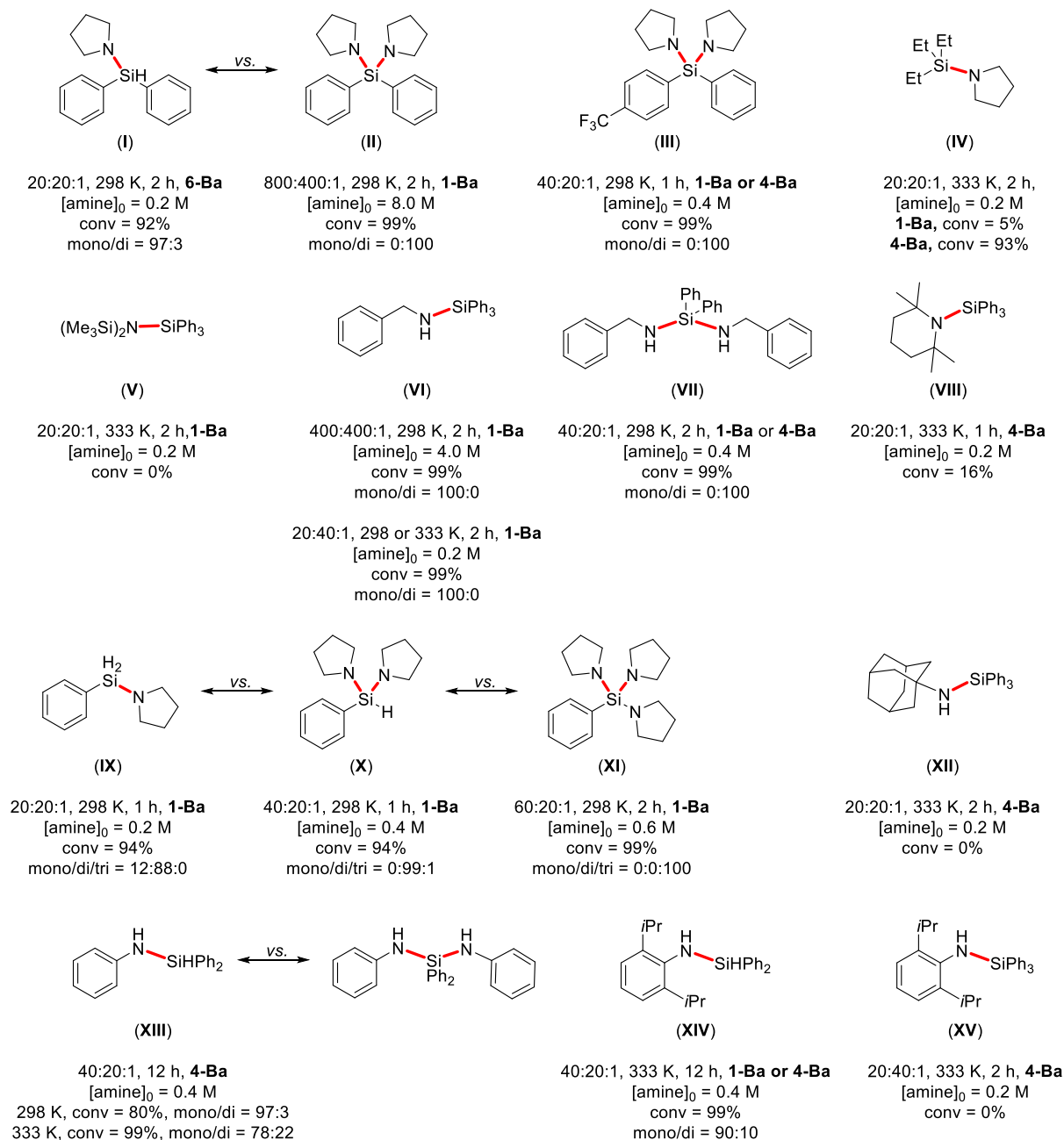
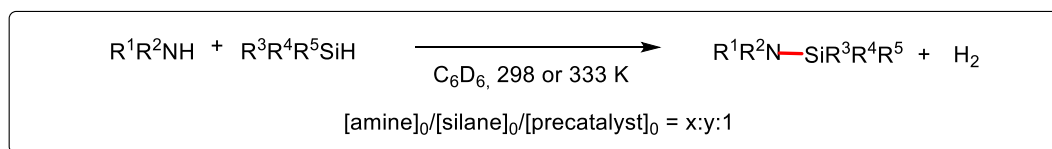
That the complexes **3-Ba** and **7-Ba** bearing a tetramethyldisilazide moiety display very poor performance is disappointing, but not entirely unexpected. Similar observations were made before with the related calcium complex $\{\text{LO}\}\text{CaN}(\text{SiMe}_2\text{H})_2 \cdot (\text{THF})$ complex ($\{\text{LO}\}^- \equiv$ aminoether-phenolato ligand) for the catalysis of intramolecular hydroamination.^[27] It was then demonstrated that this complex reacted with 2,2-dimethylpent-4-en-1-amine ($\equiv \text{H}_2\text{NR}$) upon release of H_2 through a process of self-catalysed dehydrocoupling to yield the catalytically inactive $\{\text{LO}\}\text{CaN}(\text{SiMe}_2\text{H})(\text{SiMe}_2\text{NHR})_x$. One can assume that a similar process of deactivation is occurring in the present situation with **3-Ba** and **7-Ba**, especially because of the nature of the catalysed reaction under investigation here.

Reaction scope

The substrate scope of the catalysed reaction was evaluated using precatalysts **1-Ba** and **4-Ba** (the heteroleptic and less active **6-Ba** was only used twice in specific cases for very reactive substrates) and a variety of silanes and amines. The results for this screening are summarised in Scheme 2 for reactions involving monoamines and mono(hydrosilane)s, while the coupling of di(hydrosilane)s with monoamines and that of diamines with mono(hydrosilane)s are collected in Schemes 3 and 4, respectively.^[32] The reactions were performed in C_6D_6 (identical outcomes were obtained for reactions carried out in $\text{C}_6\text{D}_5\text{Cl}$ and in 5:1 mixtures of C_6D_6 and 1,2- $\text{C}_6\text{H}_4\text{F}_2$, which present higher dielectric constants than C_6D_6)^[33] and substrate

conversion was monitored by ^1H NMR spectroscopy; all new products were characterised by standard analytical methods (^1H , ^{13}C and ^{29}Si NMR spectroscopy, mass spectrometry). Generally speaking, the chemoselectivity and measured conversions were excellent and, in the case of potentially difunctional substrates, the course of the reaction and specific formation of a given product could be controlled by judicious choice of the precatalyst (the more active **4-Ba** was used for more reluctant reactions and/or substrates) and experimental conditions (*i.e.* temperature, reaction time, substrate loading).

Arylhydrosilanes, be it Ph_3SiH , Ph_2SiH_2 or PhSiH_3 , react very quickly with pyrrolidine (Scheme 2). The dihydrosilane Ph_2SiH_2 selectively yields $\text{Ph}_2\text{SiH}(\text{N}(\text{CH}_2)_4)$ (**I**) or $\text{Ph}_2\text{Si}(\text{N}(\text{CH}_2)_4)_2$ (**II**) depending on the reactions conditions; the corresponding TON (up to 800 equiv of amine *per* metal) are otherwise unmatched. With **1-Ba** as a precatalyst, PhSiH_3 leads to the facile formation of $\text{PhSiH}(\text{N}(\text{CH}_2)_4)_2$ (**X**) or even to the tricoupled $\text{PhSi}(\text{N}(\text{CH}_2)_4)_3$ (**XI**), but the high reactivity of the PhSiH_3 /pyrrolidine pair of substrates precludes clean formation of the monocoupled product $\text{PhSiH}_2(\text{N}(\text{CH}_2)_4)$ (**IX**). The presence of an electron-withdrawing group in *para* position increases reaction rates, as seen with (*p*- $\text{CF}_3\text{-C}_6\text{H}_4$) $\text{PhSi}(\text{N}(\text{CH}_2)_4)_2$ (**III**) for which complete conversion is achieved within 1 h (compare to the formation of **I** and **II**); this observation will be discussed in more detail in the kinetic and mechanistic analysis of this catalysed process (*vide infra*). Benzylamine is as good a substrate as pyrrolidine, with high chemoselectivity, turnover numbers and reaction rates being achieved at 298 K to afford $(\text{C}_6\text{H}_5\text{CH}_2\text{NH})\text{SiPh}_3$ (**VI**) and $(\text{C}_6\text{H}_5\text{CH}_2\text{NH})_2\text{SiPh}_2$ (**VII**). Such level of selectivity is remarkable, and the formation of the *N*-dicoupled product $(\text{C}_6\text{H}_5\text{CH}_2)\text{N}(\text{SiPh}_3)_2$ was never observed. This suggests the limited ability of $(\text{SiR}_3)_x\text{NH}_{3-x}$ silazanes ($x = 1, 2$) to engage in CDC with hydrosilanes, a reckoning already made during the preliminary screening (*vide supra*) and further reinforced by the complete absence of formation of **V** in the attempted catalysed coupling of Ph_3SiH and $\text{HN}(\text{SiMe}_3)_2$.

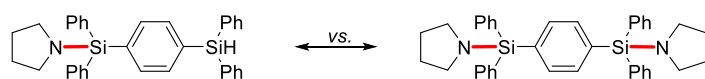
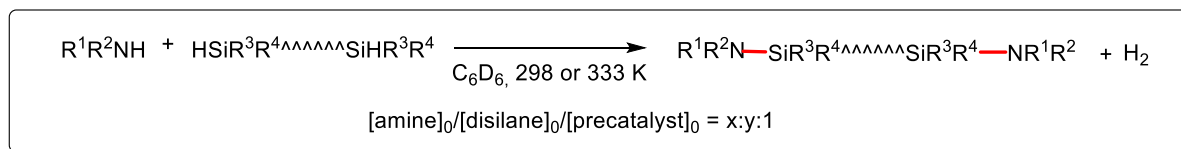


Scheme 2. Barium-catalysed cross-dehydrogenative coupling of mono(amine)s and mono(hydrosilane)s. Reactions in C₆D₆, using precatalysts **1-Ba**, **4-Ba** or **6-Ba**. For each product (**I–XV**) are indicated the [amine]₀/[silane]₀/[precat]₀ contents, reaction temperature and time, precatalyst, substrate conversion (related to the conversion of the initial hydrosilane) and chemoselectivity between mono-, di- and trisilazane products. Newly-formed bonds in red.

Aliphatic silanes are moderately reactive. The making of $\text{Et}_3\text{Si}(\text{N}(\text{CH}_2)_4)$ (**IV**) from triethylhydrosilane and pyrrolidine requires forcing conditions, even with **4-Ba**. Bulky amines also react with great difficulty. With 2-adamantylamine (\equiv adam-NH₂), no conversion to (adam-NH)SiPh₃ (**XII**) was detected spectroscopically, while CDC of tetramethylpiperidine with Ph₃SiH to yield **VIII** only reached 16% conversion after 1 h at 333 K. Aromatic amines exhibit lower reactivity than aliphatic ones, most presumably on account of their reduced nucleophilicity. Hence, 2,6-diisopropylaniline can be paired with Ph₂SiH₂ to give (2,6-*i*Pr₂-C₆H₃-NH)SiHPh₂ (**XIV**) with good selectivity after prolonged reaction time at 333K, but the corresponding coupling with the bulkier Ph₃SiH to generate **XV** failed entirely. The reactions with the less encumbered aniline proceed more smoothly. Starting from a 40:20 mixture of aniline and Ph₂SiH₂, clean formation of (C₆H₅N)SiHPh₂ (**XIII**) is achieved at 298 K, while a 78:22 mixture of **XIII** and its dicoupled derivative (C₆H₅N)₂SiPh₂ is obtained at 333 K; clean synthesis of this last product could not be achieved under the chosen experimental conditions.

The reactivity of di(hydrosilane)s follows that detailed for mono(hydrosilane)s, and gives access to original di(silazanes)s (Scheme 3). Hence, 1,2-bis(dimethylsilyl)ethane is rather unreactive. It undergoes CDC with pyrrolidine only after 12-15 h and preferably at 333 K to give mixtures of ((CH₂)₄N)(Me)₂SiCH₂CH₂SiH(Me)₂ (**XVIII**) and preponderantly its dicoupled analogue ((CH₂)₄N)(Me)₂SiCH₂CH₂Si(Me)₂(N(CH₂)₄) (**XIX**) with limited selectivity, even with precatalyst **4-Ba**. Greater reactivity is seen for 1,4-bis(diphenylsilyl)benzene, which under mild conditions couples twice with pyrrolidine or benzylamine to produce ((CH₂)₄N)(Ph₂)Si-C₆H₄-Si(Ph)₂(N(CH₂)₄) (**XVI**) and (C₆H₅CH₂N)SiPh₂-C₆H₄-SiPh₂(NCH₂C₆H₅) (**XVII**), respectively, with good chemoselectivity. The reactivity of 1,4-bis(dimethylsilyl)benzene towards pyrrolidine is also rather satisfactory: **1-Ba** and **4-Ba** both afford clean access to

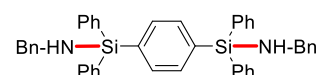
$((\text{CH}_2)_4\text{N})(\text{Me})_2\text{Si}-\text{C}_6\text{H}_4-\text{Si}(\text{Me})_2(\text{N}(\text{CH}_2)_4)$ (**XXI**), while **6-Ba** allows the preponderant formation of the monocoupled derivative, $((\text{CH}_2)_4\text{N})\text{SiMe}_2-\text{C}_6\text{H}_4-\text{SiMe}_2\text{H}$ (**XX**).



(XVI)

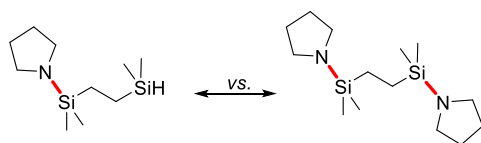
40:20:1, 298 K, 2 h, **4-Ba**
 [amine]₀ = 0.4 M
 conv = 99%
 mono/di = 6:94

40:20:1, 298 K, 2 h, **1-Ba**
 [amine]₀ = 0.4 M
 conv = 90%
 mono/di = 10:90



(XVII)

40:20:1, 298 K, 2 h, **1-Ba** or **4-Ba**
 [amine]₀ = 0.4 M
 conv = 99%
 mono/di = 0:100



(XVIII)

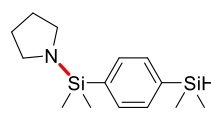
20:20:1, 333 K, 15 h, **1-Ba**
 [amine]₀ = 0.2 M
 conv = 80%
 mono/di = 49:51

(XIX)

40:20:1, 298 K, 2 h, **4-Ba**
 [amine]₀ = 0.4 M
 conv = 89%
 mono/di = 36:64

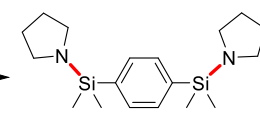
40:20:1, 333 K, 2 h, **4-Ba**
 [amine]₀ = 0.4 M
 conv = 99%
 mono/di = 10:90

40:20:1, 333 K, 6 h, **1-Ba**
 [amine]₀ = 0.4 M
 conv = 75%
 mono/di = 30:70



(XX)

40:20:1, 298 K, 2 h, **6-Ba**
 [amine]₀ = 0.4 M
 conv = 99%
 mono/di = 90:10



(XXI)

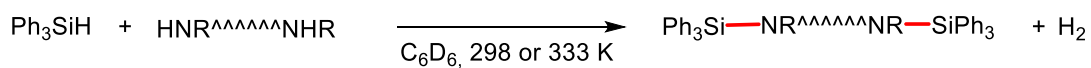
40:20:1, 298 K, 2 h, **4-Ba**
 [amine]₀ = 0.4 M
 conv = 99%
 mono/di = 0:100

40:20:1, 298 K, 2 h, **1-Ba**
 [amine]₀ = 0.4 M
 conv = 99%
 mono/di = 31:69

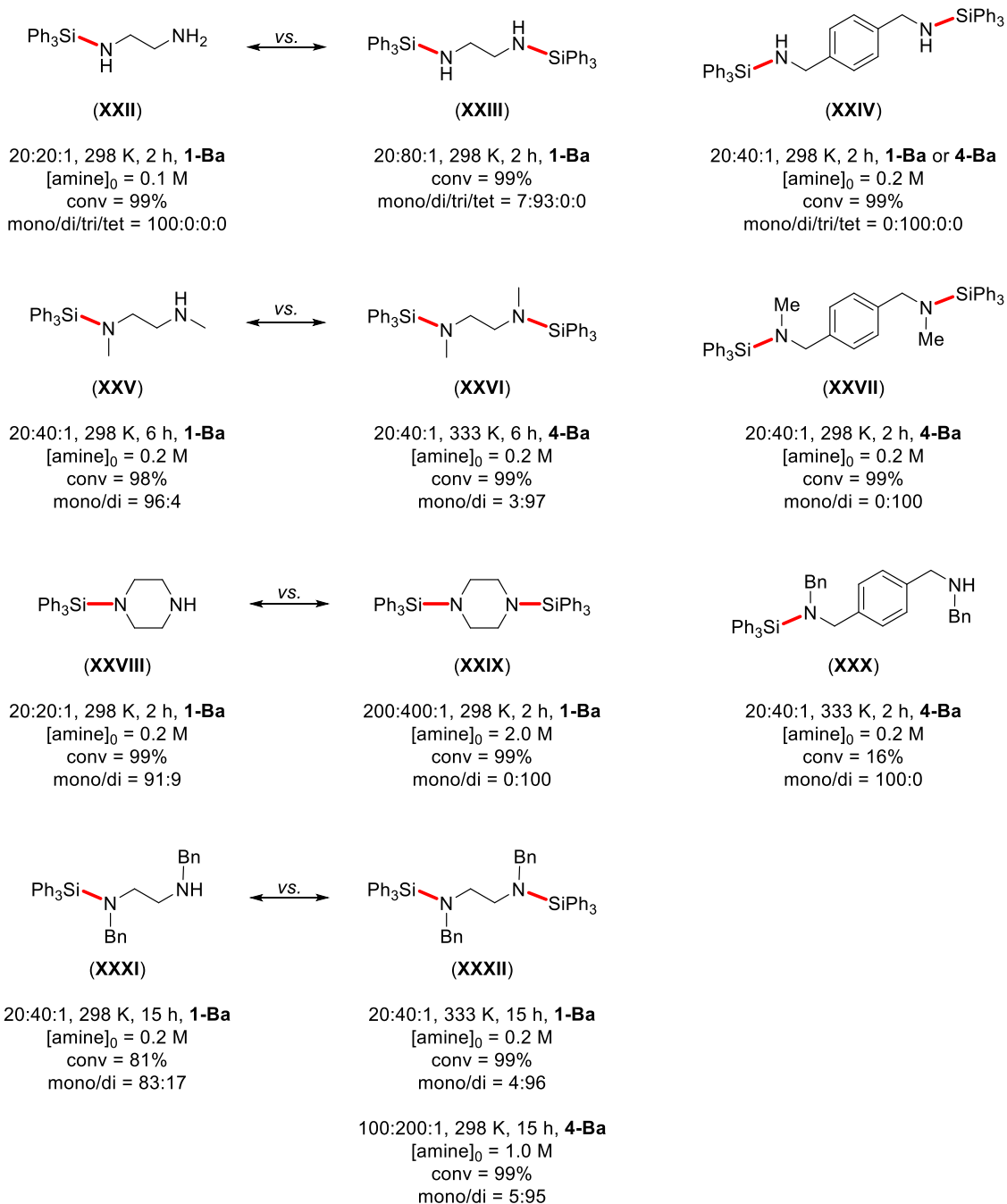
40:20:1, 333 K, 15 h, **1-Ba**
 [amine]₀ = 0.4 M
 conv = 99%
 mono/di = 3:97

Scheme 3. Barium-catalysed CDC of amines and disilanes. Reactions carried out in C₆D₆, using precatalysts **1-Ba**, **4-Ba** or **6-Ba**. For each product (**XVI–XXI**) are indicated the [amine]₀/[disilane]₀/[precat]₀ contents, reaction temperature and time, precatalyst, substrate conversion (related to the conversion of the initial di(hydrosilane)) and chemoselectivity between mono-, di- and tri-silazane products. Newly-formed bonds in red.

The utilisation of diamines leads to the formation of valuable di(silazane)s (Scheme 4). Starting from 1,2-ethylenediamine, the reaction can be oriented towards the formation of $\text{Ph}_3\text{SiNHCH}_2\text{CH}_2\text{NH}_2$ (**XXII**) or $\text{Ph}_3\text{SiNHCH}_2\text{CH}_2\text{NHSiPh}_3$ (**XXIII**) depending on the initial contents in Ph_3SiH ; in no case was further coupling to $(\text{Ph}_3\text{Si})_2\text{NCH}_2\text{CH}_2\text{NHSiPh}_3$ or even $(\text{Ph}_3\text{Si})_2\text{NCH}_2\text{CH}_2\text{N}(\text{SiPh}_3)_2$ observed, another indication that $-\text{NHSiR}_3$ silazanes engage in CDC with hydrosilanes at best with great difficulty. From a same N,N' -dimethylethylenediamine/ Ph_3SiH feed ratio of 20:40, precatalysts **1-Ba** (at 298 K) and **4-Ba** (at 333 K) yield respectively the monocoupled $\text{Ph}_3\text{Si}(\text{Me})\text{NCH}_2\text{CH}_2\text{NHMe}$ (**XXV**) and $\text{Ph}_3\text{Si}(\text{Me})\text{NCH}_2\text{CH}_2\text{N}(\text{Me})\text{SiPh}_3$ (**XXVI**). Similarly, on adjusting the initial hydrosilane contents, the CDC of Ph_3SiH with piperazine at 298 K catalysed by **1-Ba** readily affords the mono- and the dicoupled products **XXVIII** or **XXIX** with high chemoselectivity. By pairing N,N' -dibenzylethylenediamine with Ph_3SiH , one gets access to $\text{Ph}_3\text{Si}(\text{Bn})\text{NCH}_2\text{CH}_2\text{NHBn}$ (**XXXI**) and $\text{Ph}_3\text{Si}(\text{Bn})\text{NCH}_2\text{CH}_2\text{N}(\text{Bn})\text{SiPh}_3$ (**XXXII**), although the selectivity towards **XXXI** was only moderate (83%). Diamines such as 1,4-phenylenedimethanamine and its N,N' -dimethyl substituted congeners display mixed reactivity towards with Ph_3SiH . The dicoupled $\text{Ph}_3\text{SiHNCH}_2-\text{C}_6\text{H}_4-\text{CH}_2\text{NHSiPh}_3$ (**XXIV**) and $\text{Ph}_3\text{Si}(\text{Me})\text{NCH}_2-\text{C}_6\text{H}_4-\text{CH}_2\text{N}(\text{Me})\text{SiPh}_3$ (**XXVII**) could be obtained under smooth conditions with excellent selectivity. However, $\text{BnHNCH}_2-\text{C}_6\text{H}_4-\text{CH}_2\text{NHBn}$ is far less reactive, leading to the exclusive formation of the monocoupled $\text{Bn}(\text{Ph}_3\text{Si})\text{NCH}_2-\text{C}_6\text{H}_4-\text{CH}_2\text{NHBn}$ (**XXX**) but in poor yield (16%), even at 333 K with **4-Ba**.^[34]



$$[\text{diamine}]_0/[\text{silane}]_0/[\text{precatalyst}]_0 = x:y:1$$



Scheme 4. Barium-catalysed CDC of diamines and triphenylsilane. Reactions carried out in C₆D₆, using precatalysts **1-Ba** or **4-Ba**. For each product (**XXII–XXXII**) are indicated the [diamine]₀/[silane]₀/[precat]₀ contents, reaction temperature and time, precatalyst, substrate conversion (related to the conversion of the initial di(amine)) and chemoselectivity between mono-, di- and tri-silazane products. Newly-formed bonds in red.

Overall, the barium precatalysts **1-Ba** and **4-Ba** display a remarkable combination of productivity, activity and chemoselectivity in N–H/H–Si CDC reactions, and give access to a wide panel of original mono- and disilazanes. Of particular interest, several of these products still possess N–H and/or Si–H reactive functional groups, rendering them useful synthetic intermediates which can be used for further functionalisation reactions. The performance displayed by **1-Ba** and **4-Ba** in the CDC of ditopic diamines and dihydrosilanes or di(hydrosilane)s suggests that they could make good precatalysts for dehydrogenative polymerisation to afford poly(carbosilazane)s, and indeed we have for instance been able to prepare low molecular weight polymers ($M_n = 3\text{--}6.10^3 \text{ g mol}^{-1}$) from *N,N'*-dibenzylethylenediamine and Ph_2SiH_2 .^[32]

Kinetic analysis

Kinetic investigations were carried out to improve our understanding of these Ae-mediated N–H–/H–Si CDC reactions. The main lines of the analysis of the coupling of pyrrolidine with triphenylsilane, our benchmark substrates, catalysed by the bulky amido **6-Ba** (a precatalyst less active than **1-Ba** and **4-Ba** and which lends itself well to the monitoring of substrate conversion by ¹H NMR spectroscopy) were reported in our early communication.^[20c] They are recalled here, together with comparative data for Ca, Sr and Ba precatalysts.

From reactions carried out in C_6D_6 at 298 K and aimed at investigating the influence of the concentrations in substrates (with $[\text{pyrrolidine}]_0$ or $[\text{triphenylsilane}]_0$ varying over a 21-fold concentration range, Figures 3 and 4) and precatalyst ($[\text{6-Ba}]_0$ studied over a 15-fold concentration range, Figure 5), the second-order rate law

$$R = -d[\text{pyrrolidine}]/dt = k [\text{6-Ba}]^1 [\text{pyrrolidine}]^0 [\text{triphenylsilane}]^1 \quad (1)$$

was established, with $k = 4.802(13) \times 10^{-3} \text{ M}^{-1} \text{ s}^{-1}$. An identical kinetic rate law was reported by Sadow and co-workers for N–H/H–Si dehydrocoupling reactions catalysed by

$\{\text{To}^{\text{M}}\}\text{Mg}(\text{N}(\text{SiMe}_3)_2)$.^[20a] On the other hand, it is different from the rate laws given by Hill and co-workers for the bis-amido precatalysts $\{\text{Ae}[\text{N}(\text{SiMe}_3)_2]_2\}_2$, which were found to be $R = k \cdot [\text{Ae}]^1 \cdot [\text{pyrrolidine}]^1 \cdot [\text{triphenylsilane}]^0$ for $\text{Ae} = \text{Mg}$ and Ca , and $R = k \cdot [\text{Ae}]^2 \cdot [\text{pyrrolidine}]^1 \cdot [\text{triphenylsilane}]^1$ for $\text{Ae} = \text{Mg}$ and Ca .^[20b] For experiments run under otherwise identical conditions, a strong kinetic isotopic effect of $k_{\text{Ph}_3\text{SiH}}/k_{\text{Ph}_3\text{SiD}} = 4.7(1)$ was measured for the coupling of Ph_3SiX ($\text{X} = \text{H}$, duplicated experiments; D , triplicated experiments; the mean values of $k_{\text{Ph}_3\text{SiH}}$ and $k_{\text{Ph}_3\text{SiD}}$ were used to obtain the KIE) and $\text{HN}(\text{CH}_2)_4$ (Figure 6), *i.e.* within the accuracy of the methods it is commensurate with the maximal theoretical value.^[35] No substantial kinetic effect was detected for the amine, $k_{\text{HN}(\text{CH}_2)_4}/k_{\text{DN}(\text{CH}_2)_4} = 1.0(1)$. Both findings are consistent with the kinetic rate law, and clearly implicate that only the rupture of the Si–H bond intervenes as a key event of the turnover limiting step.

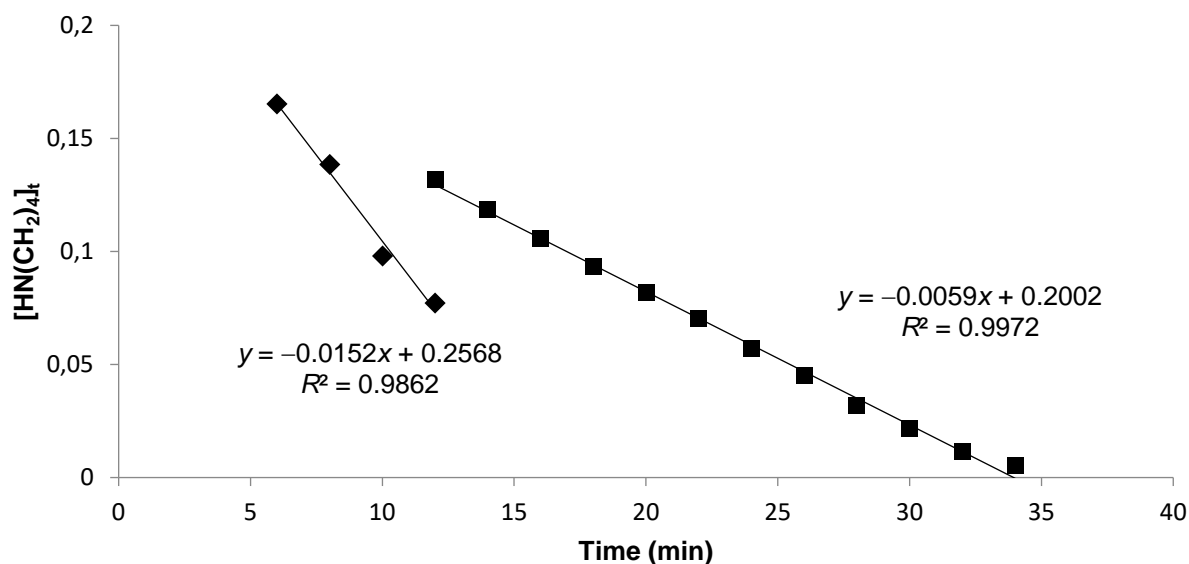


Figure 3. Plot of $[\text{HN}(\text{CH}_2)_4] = k_{\text{obs}} \cdot t$ as a function of time for the CDC of pyrrolidine and Ph_3SiH catalysed by **6-Ba**, showing a partial kinetic zeroth-order in $[\text{pyrrolidine}]$. Conditions: $\text{HN}(\text{CH}_2)_4$ ($8.0 \mu\text{L}$, 0.1 mmol), Ph_3SiH (300 mg , 1.15 mmol), $[\mathbf{6-Ba}]_0 = 0.0179 \text{ M}$ (♦, $k_{\text{obs}} = 2.53 \times 10^{-4} \text{ s}^{-1}$) or 0.0097 M (■, $k_{\text{obs}} = 9.83 \times 10^{-5} \text{ s}^{-1}$), $T = 298 \text{ K}$, solvent C_6D_6 .

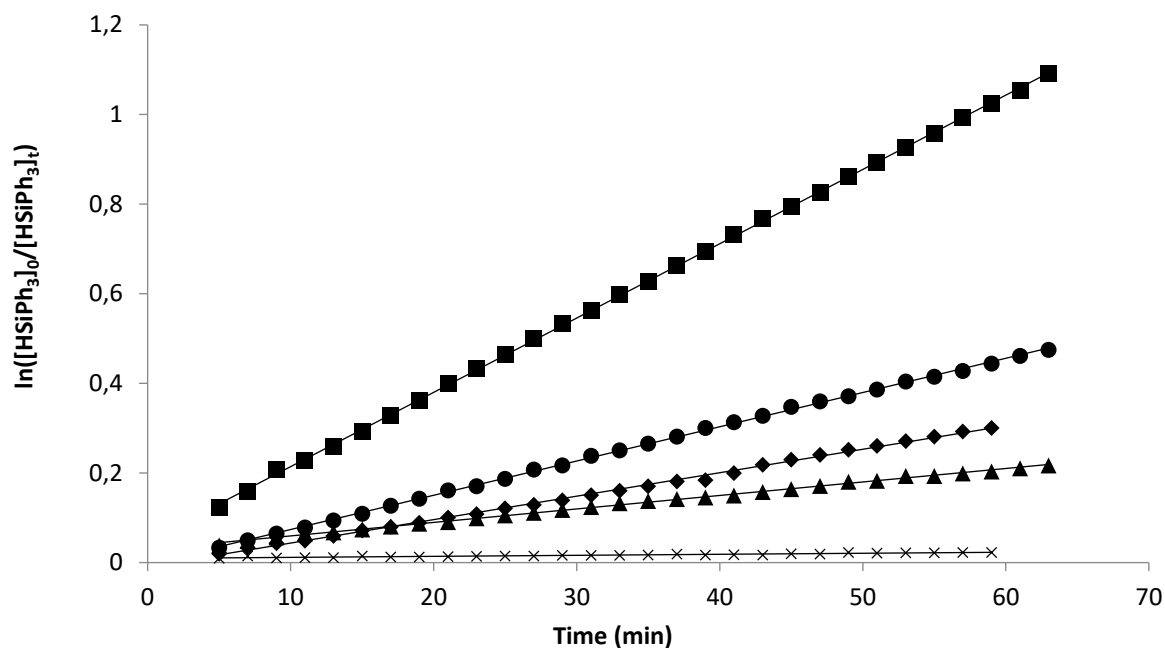


Figure 4. Plot of $\ln([\text{HSiPh}_3]_0/[\text{HSiPh}_3]_t) = k_{\text{obs}}.t$ as a function of time for the CDC of pyrrolidine and Ph_3SiH catalysed by **6-Ba**, indicating a partial kinetic first-order in [triphenylsilane]. $T = 298 \text{ K}$, solvent C_6D_6 , $\text{HN}(\text{CH}_2)_4$ ($160 \mu\text{L}$, 2.0 mmol), HSiPh_3 (10.0 mg , 0.04 mmol), with $[\text{6-Ba}] = 4.0 \text{ mM}$ (\times , $k_{\text{obs}} = 3.33 \times 10^{-6} \text{ s}^{-1}$), 11.0 mM (\blacktriangle , $k_{\text{obs}} = 4.67 \times 10^{-5} \text{ s}^{-1}$), 26.0 mM (\blacklozenge , $k_{\text{obs}} = 8.67 \times 10^{-5} \text{ s}^{-1}$), 30.0 mM (\bullet , $k_{\text{obs}} = 1.27 \times 10^{-4} \text{ s}^{-1}$) and 60.0 mM (\blacksquare , $k_{\text{obs}} = 2.77 \times 10^{-4} \text{ s}^{-1}$).

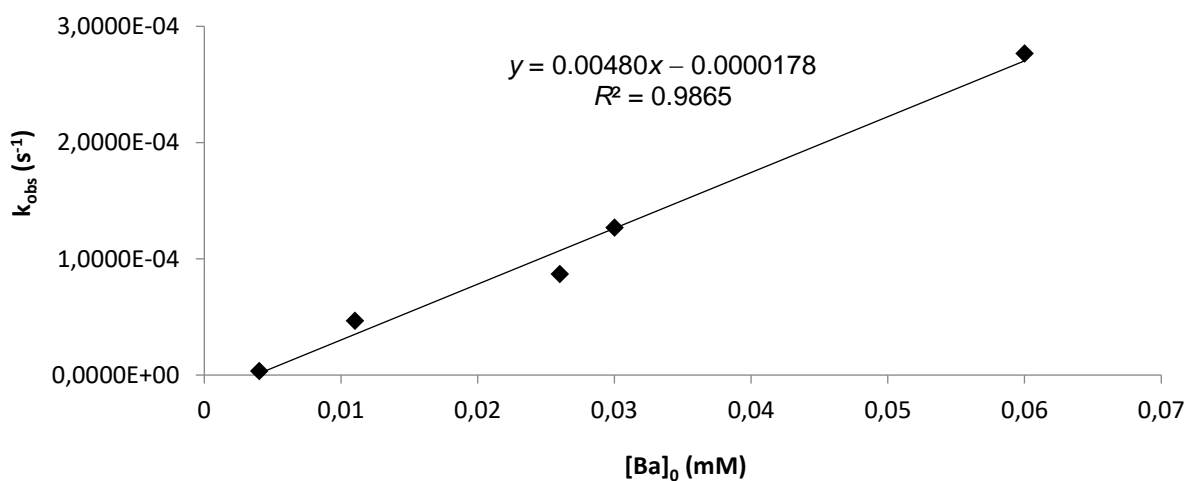


Figure 5. Linear plot of $k_{\text{obs}} = k.[\text{6-Ba}]$ as a function of $[\text{Ba}]_0$ for the CDC of pyrrolidine and Ph_3SiH catalysed by **6-Ba**, showing a partial kinetic first-order in **6-Ba** with $k = 4.80 \times 10^{-3} \text{ M}^{-1}.\text{s}^{-1}$. Conditions: $\text{HN}(\text{CH}_2)_4$ ($160 \mu\text{L}$, 2.0 mmol), HSiPh_3 (10 mg , 0.04 mmol), with $[\text{6-Ba}] = 4.0, 11.0, 26.0, 30.0$ and 60.0 mM , $T = 298 \text{ K}$, solvent C_6D_6 .

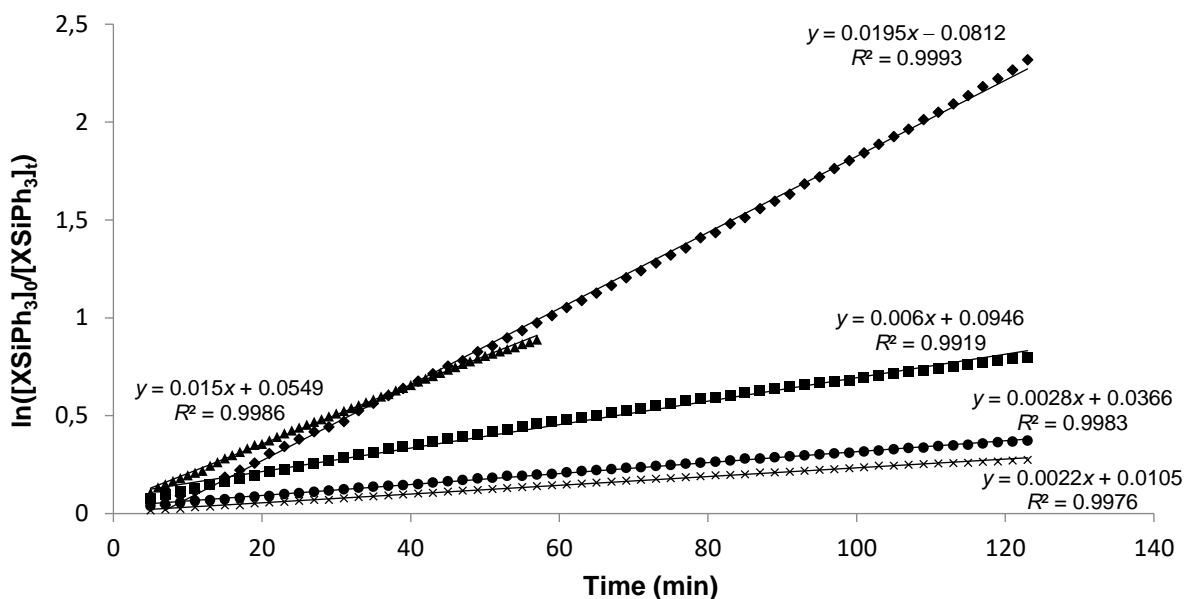


Figure 6. Plot of $\ln([XSiPh_3]_0/[XSiPh_3]_t) = k_{obs} \cdot t$ as a function of time for X = H or D for the CDC of pyrrolidine and Ph_3SiH catalysed by **6-Ba**. Conditions: $HN(CH_2)_4$ (12.0 μL , 0.15 mmol), $HSiPh_3$ or $DSiPh_3$ (39 mg, 0.15 mmol) and **6-Ba** (4.4 mg, 5.0 μmol), $T = 298$ K, solvent C_6D_6 . $HSiPh_3$ (\blacklozenge , \blacktriangle), $k_{obs} = 3.25 \times 10^{-4}$ and $2.50 \times 10^{-4} s^{-1}$; $DSiPh_3$ (\blacksquare , \bullet and \times), $k_{obs} = 1.00 \times 10^{-4}$, $4.67 \times 10^{-5} s^{-1}$ and $3.67 \times 10^{-5} s^{-1}$.

The activation parameters $\Delta H^\ddagger = 15.6(23) \text{ kcal mol}^{-1}$ and $\Delta S^\ddagger = -13.3(7.5) \text{ cal mol}^{-1} \text{ K}^{-1}$ ($\Delta G_{298}^\ddagger = 19.6(1) \text{ kcal mol}^{-1}$ at 298 K) were determined by an Eyring analysis, using 6 data points in the temperature range 293–318 K (Figure 7).^[36] The negative value of ΔS^\ddagger , diagnostic of an associative mechanism, is small in view of those given for other Mg–Sr CDC precatalysts;^[20a-b] this is possibly a consequence of the large radius of the Ba^{2+} ion ($r_{ionic} = 1.38 \text{ \AA}$) which may induce a less constrained arrangement in the transition state.

A Hammett analysis was performed on the coupling of pyrrolidine with $Ph_2(p\text{-X-C}_6\text{H}_4)\text{SiH}$, with X chosen amongst Me, OMe, F and CF_3 at the *para* position of one of the aromatic moieties in the triarylsilanes. It showed that in comparison with Ph_3SiH (X = H), the reaction rates increased very substantially with electron-withdrawing groups (X = F, CF_3) and decreased with electron-donating ones (X = Me, OMe), with a variation according to $X = OMe < Me < H < F < CF_3$ (Table 2). The Hammett plot $\ln(k_H/k_X) = \sigma_p(X) \cdot \rho$ is a straight line with a positive slope of $\rho = 2.0(2)$ (Figure 8),^[37] clearly indicating that the activation

barrier of the catalytic event is lowered by *para* electron-withdrawing, presumably through stabilisation of a developing negative charge on the silicon atom. This is consistent with the finding that the catalysed reaction leading to the formation of (*p*-CF₃-C₆H₄)PhSi(N(CH₂)₄)₂ (**III**) is more rapid than those yielding PhSiH(N(CH₂)₄)₂ (**I**) and Ph₂Si(N(CH₂)₄)₂ (**II**) (see Scheme 2).

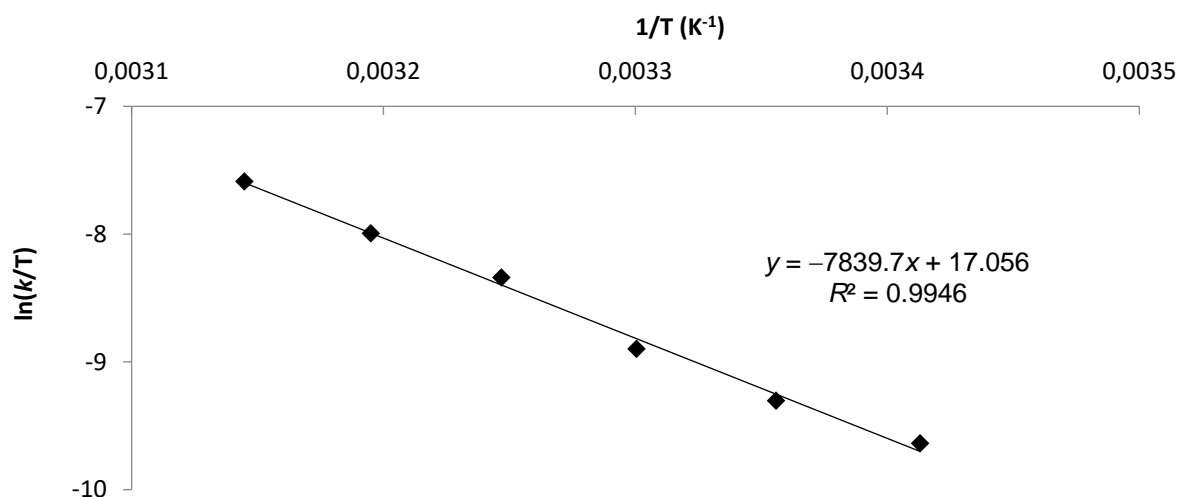


Figure 7. Eyring plot for the CDC of pyrrolidine and Ph₃SiH catalysed by **6-Ba**; k was determined from the plot of $\ln([\text{HSiPh}_3]_0/[\text{HSiPh}_3]_t) = k_{\text{obs}} \cdot t$ with $k_{\text{obs}} = k \cdot [\mathbf{6-Ba}]^1 [\text{HN}(\text{CH}_2)_4]^0$. HN(CH₂)₄ (8.0 μL, 0.10 mmol), HSiPh₃ (26 mg, 0.10 mmol) and **6-Ba** (3.0 mg, 0.0034 mmol), solvent C₆D₆, Temperature range: 293–318 K.

Table 2. Hammett analysis for the CDC of pyrrolidine and Ph₂(*p*-X-C₆H₄)SiH, with X = H, Me, OMe, F and CF₃, catalysed by **6-Ba**^[a]

X = OMe		X = Me		X = H		X = F		X = CF ₃	
[6-Ba] ₀ [mM]	k_{obs} [10 ⁵ .s ⁻¹]	[6-Ba] ₀ [mM]	k_{obs} [10 ⁵ .s ⁻¹]	[6-Ba] ₀ [mM]	k_{obs} [10 ⁵ .s ⁻¹]	[6-Ba] ₀ [mM]	k_{obs} [10 ⁵ .s ⁻¹]	[6-Ba] ₀ [mM]	k_{obs} [10 ⁵ .s ⁻¹]
11.0	2.67	10.0	0.33	4.0	0.33	5.0	2.00	5.0	3.83
17.0	5.17	17.0	3.67	11.0	4.67	19.0	9.00	10.0	11.3
28.0	6.67	24.0	4.83	26.0	8.67	27.0	13.8	17.0	27.5
39.0	9.83	31.0	7.33	30.0	12.7	32.0	16.3	29.0	39.2
50.0	11.2	42.0	14.0	60.0	27.7	39.0	18.7	50.0	64.2

[a] Reactions in C₆D₆ (0.5 mL) at 298 K, [pyrrolidine]₀ = 3.0 M, [Ph₂(*p*-X-C₆H₄)SiH]₀ = 0.06 M.

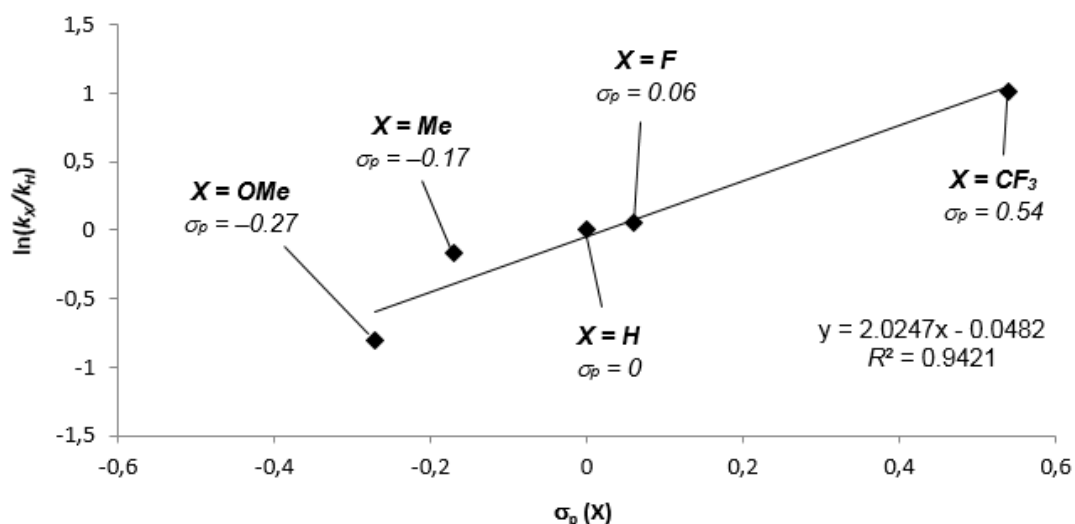


Figure 8. Hammett plot $\ln(k_H/k_X) = \sigma_p(X) \times \rho$ showing the reaction rate acceleration with electron-withdrawing groups on the silane for the coupling of $\text{HN}(\text{CH}_2)_4$ and $\text{Ph}_2(p\text{-X-C}_6\text{H}_4)\text{SiH}$ (with $X = \text{OMe}, \text{Me}, \text{H}, \text{F}, \text{CF}_3$) catalysed by **6-Ba**. Experimental conditions: solvent C_6D_6 (0.5 mL), $T = 298 \text{ K}$, $\text{HN}(\text{CH}_2)_4$ (3.0 M), $\text{Ph}_2(p\text{-X-C}_6\text{H}_4)\text{SiH}$ (0.06 M).

From the qualitative experiments performed in the preliminary precatalyst screening (see Table 1), it had emerged that the catalytic activity increased according to $\text{Ca} < \text{Sr} < \text{Ba}$. To better quantify this observation, the conversion of pyrrolidine during the CDC of pyrrolidine and triphenylsilane catalysed by **6-Ca**, **6-Sr** or **6-Ba** at 298 K was monitored by NMR spectroscopy. The observed rate constants obtained from the semi-logarithmic plot of substrate conversion *vs.* time (Figure 9) corroborate the earlier finding, that is, under the chosen experimental conditions, they increased by *ca.* one order of magnitude from calcium ($k_{\text{obs}} = 3.83 \times 10^{-5} \text{ s}^{-1}$) to strontium ($k_{\text{obs}} = 15.7 \times 10^{-5} \text{ s}^{-1}$) and to the most efficacious metal, barium ($k_{\text{obs}} = 32.5 \times 10^{-5} \text{ s}^{-1}$).

For a given ligand set, the $\text{Ca} < \text{Sr} < \text{Ba}$ activity trend has often been reported in a variety of catalytic reactions, for instance in the ring-opening polymerisation of cyclic esters,^[38] the intermolecular hydroamination and hydrophosphination of activated alkenes,^[29,39] or the hydrophosphonylation of ketones.^[40] However, this must be mitigated, as there is now for instance a large body of evidence showing that the activity varies with $\text{Ba} <$

Sr < Ca in the cyclohydroamination of aminoalkenes,^[41] while no obvious trend actually emerges in some other cases, *e.g.* for the hydroalkoxylation/cyclisation of alkynyl alcohol.^[42] The size of the alkaline-earth ion, its polarizability, electron surface potential and ability to bind incoming substrates and polarise their reactive bonds are all unquestionably some of the features that define the reactivity of the pertaining complexes and their catalytic ability.

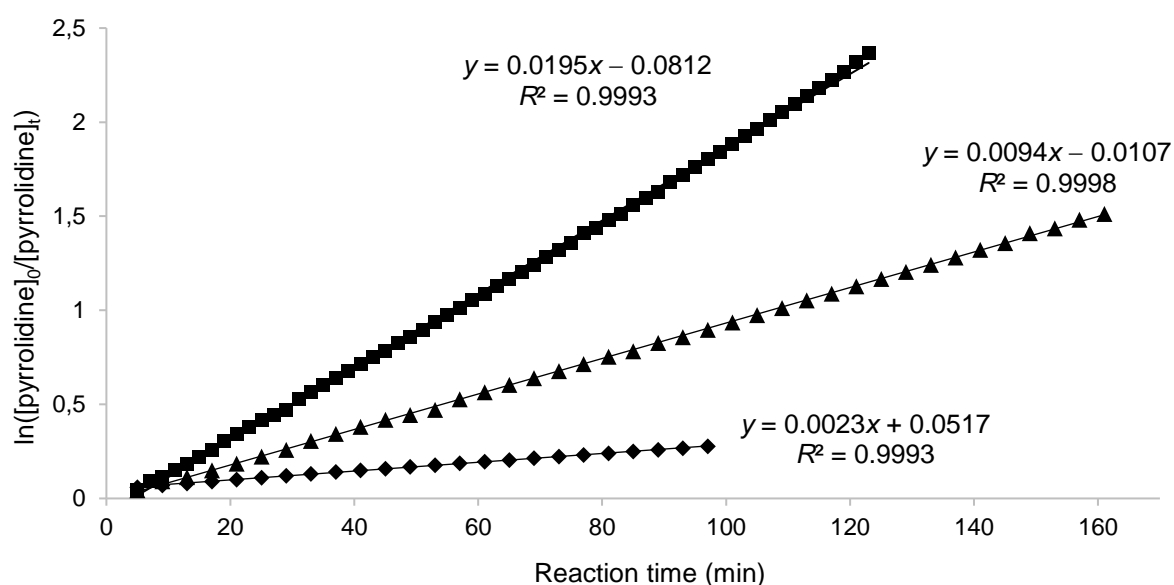


Figure 9. Comparative semi-logarithmic plot of pyrrolidine conversion vs. reaction time for the CDC of pyrrolidine with triphenylsilane catalysed by **6-Ca** (\blacklozenge , $k_{\text{obs}} = 3.83 \times 10^{-5} \text{ s}^{-1}$), **6-Sr** (\blacktriangle , $k_{\text{obs}} = 15.7 \times 10^{-5} \text{ s}^{-1}$) and **6-Ba** (\blacksquare , $k_{\text{obs}} = 32.5 \times 10^{-5} \text{ s}^{-1}$). Experimental conditions: $[\text{pyrrolidine}]_0 = 0.20 \text{ M}$, $[\text{pyrrolidine}]_0/[\text{triphenylsilane}]_0/[\text{precatalyst}]_0 = 20:20:1$, C_6D_6 (0.5 mL), $T = 298 \text{ K}$.

Computational investigations

In order to inform ourselves about which of the several conceivable mechanistic scenarios does prevail, we embarked on a detailed computational analysis of alternative pathways for the CDC of pyrrolidine (A) and Ph_3SiH (S) catalysed by $[\{\text{N}^{\wedge}\text{N}\}\text{Ba}\{\text{N}(\text{SiMe}_3)_2\} \cdot (\text{THF})_2]$ (**6-Ba**, denoted thereafter as **C2**•(T)²). Various mechanistic pathways for a barium pyrrolide (Scheme 5) or alternatively a barium silyl (Scheme 6) representing the catalytically competent compound have been thoroughly examined, the most accessible of which has been briefly

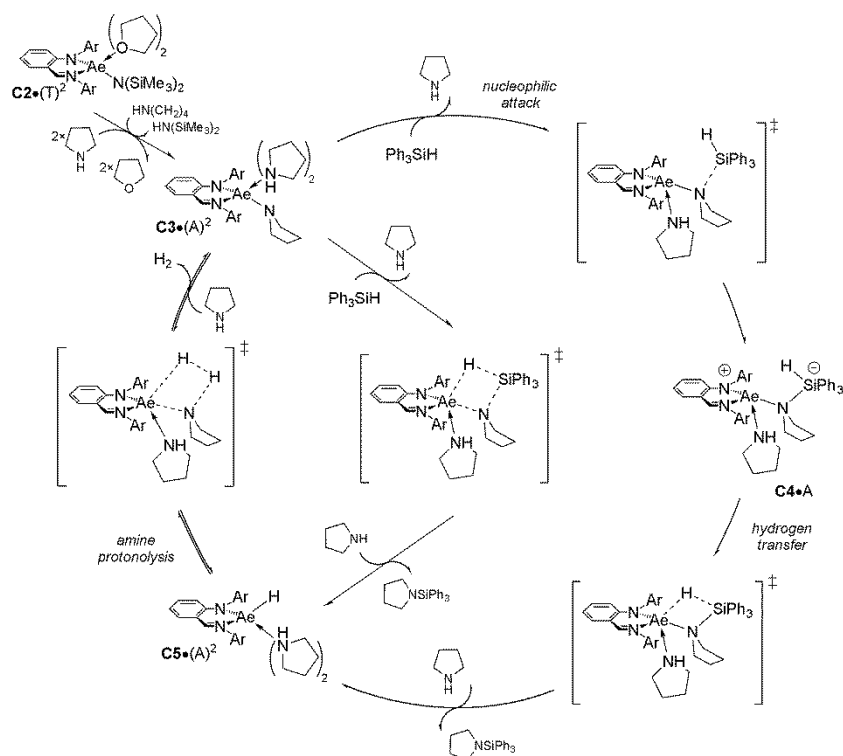
characterised in our previous communication.^[20c] Taking the route for generation of the silazane product (P) that commences from the {N[^]N}Ae pyrrolide by evolving through a {N[^]N}Ae hydride intermediate, which is converted back into the {N[^]N}Ae pyrrolide compound thereafter (Scheme 5), as an example, the aforementioned kinetic data are in support of both stepwise and concerted pathways, which further adds to the mechanistic diversity. The computational methodology employed (dispersion-corrected B97-D3 in conjunction with basis sets of triple- ζ basis sets and a sound treatment of bulk solvent effects; see the Computational Details section for more details) simulated authentic reaction conditions adequately. The validity of the computational protocol to reliably map the free-energy landscape of Ae-mediated hydroelementation reactions has been substantiated before^[39,41g] and this has allowed mechanistic conclusions with substantial predictive value to be drawn.

Herein we report the full account of examined pathways that are conceivable for delivering the silazane product and also of the disilane by-product by the barium silylamide **6-Ba** ($\equiv \mathbf{C2}\cdot(\mathbf{T})^2$). A second part scrutinizes the effect of the alkaline-earth metal (Ae = Ca, Sr) on the energetics of relevant elementary steps, thereby providing invaluable insights into crucial structure-activity relationships of the CDC mediated by alkaline-earth iminoanilides.

A – Pathways starting from the {N[^]N}Ba pyrrolide

A recent computational study^[39] of styrene hydroamination has revealed that the initial transformation of the {N[^]N}Ba silylamide $\mathbf{C2}\cdot(\mathbf{T})^2$ precursor into the {N[^]N}Ba pyrrolide compound **C3**, which is predominantly present as the bis(amine) adduct $\mathbf{C3}\cdot(\mathbf{A})^2$ and exhibits no propensity towards forming dimers, is sufficiently facile kinetically. As far as catalytically competent silane adducted species ($\mathbf{C3}\cdot\mathbf{S}\cdot(\mathbf{A})^n$) are concerned, a single adducted amine molecule stabilizes $\mathbf{C3}\cdot\mathbf{S}$ greatly, whereas the presence of the rather bulky Ph₃SiH makes it

impossible for the $\{N^{\wedge}N\}Ba$ centre to accommodate another pyrrolidine molecule. Hence, $C3 \cdot S$ and its mono-amine adducted species $C3 \cdot S \cdot A$ are likely to be participating in accessible pathways for catalyst turnover.



Scheme 5. Plausible mechanistic pathways for iminoanilide alkaline-earth-catalysed CDC of amines and silanes with $\{[N^{\wedge}N]Ae\{N(CH_2)_4\}\}$ ($C3$) as the catalytically competent compound and triphenylsilane (S) and pyrrolidine (A) substrates ($\{N^{\wedge}N\}^- = [ArN(o-C_6H_4)C(H)=NAr]^-$ with $Ar = 2,6-iPr-C_6H_3$).

We start with the examination of a stepwise pathway (Scheme 5) for silazane formation comprising nucleophilic attack of the $\{N^{\wedge}N\}Ae$ pyrrolide at the silane to furnish the transient silicate intermediate $C4$ and subsequent hydrogen transfer to the alkaline earth, thereby giving rise to the $\{N^{\wedge}N\}Ae$ hydride $C5$ with the release of the silazane product P. The initial nucleophilic attack of a suitably nucleophilic pyrrolide N centre at S commencing from $C3 \cdot S$ or $C3 \cdot S \cdot A$, featuring an only loosely associated silane molecule, evolves through a transition state (TS) structure describing N–Si bond formation to occur outside of the immediate vicinity of the alkaline earth at distances of 2.40–2.50 Å (see Figure S1 in the

Supporting Information) for the emerging N–Si bond. Following the reaction path further, TS structures decay into a metastable nucleophilic $\{N^{\wedge}N\}$ Ba silicate intermediate **C4**, featuring a five-coordinate silicon centre with an already elongated Si–H linkage, thus indicating its distinct aptitude to undergo β -H elimination. No substantial structural reorganisation is required for the transfer of the hydrogen from the five-coordinate silicon onto the alkaline earth to proceed through a TS structure with distances of approximately 2.45 and 2.40 Å for vanishing Si–H and emerging Ba–H bonds (see Figure S1 in the Supporting Information), respectively, thereby generating the silazane product and $\{N^{\wedge}N\}$ Ba hydride **C5**.

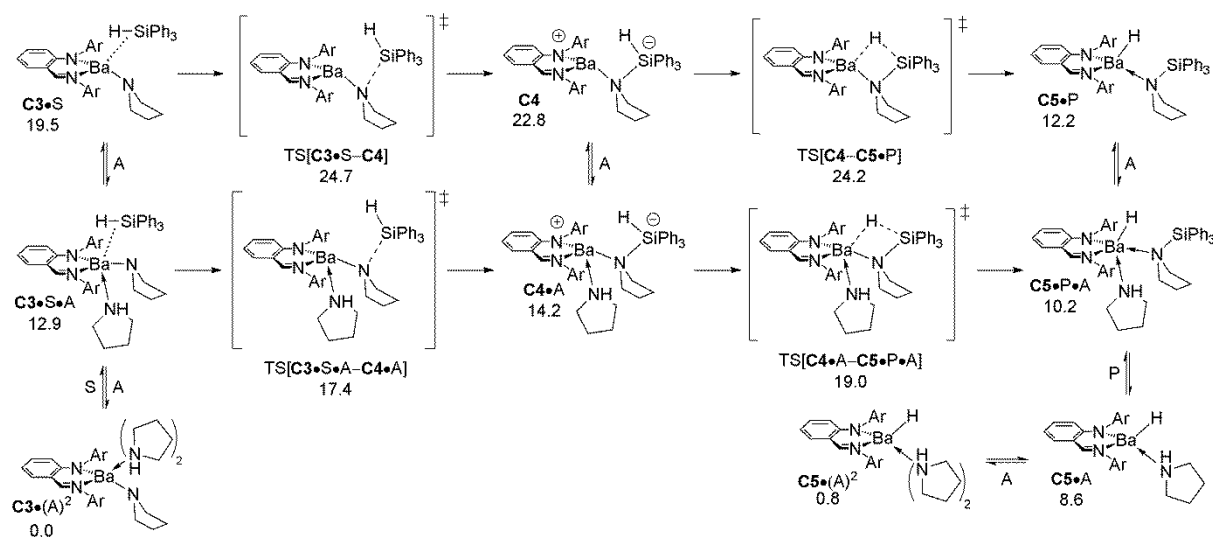


Figure 10. Nucleophilic attack of the $\{N^{\wedge}N\}$ Ba pyrrolide **C3** at the triphenylsilane **S** together with subsequent hydrogen transfer to barium at the transient silicate intermediate **C4** to afford $\{N^{\wedge}N\}$ Ba hydride **C5** and the silazane (**P**) product.^[43,44a]

The most accessible pathway for the stepwise silazane generation benefits from one associated pyrrolidine spectator molecule to participate at all stages of the process (**C3•S•A**→**C4•A**→**C5•P•A**) on both kinetic and thermodynamic grounds (Figure 10). As far as the intrinsic reactivity is concerned, both the N–Si bond-forming nucleophilic attack of the Ba pyrrolide ($\Delta G^{\ddagger}_{\text{int}} = 4.5 \text{ kcal mol}^{-1}$ relative to **C3•S•A**) and the hydrogen transfer ($\Delta G^{\ddagger}_{\text{int}} = 4.8 \text{ kcal mol}^{-1}$ relative to **C4•A**) are seen to be feasible kinetically to an astonishingly

comparable amount. In terms of observable catalytic performance, the nucleophilic attack is predicted to be kinetically affordable ($\Delta G^\ddagger = 17.4 \text{ kcal mol}^{-1}$ relative to $\mathbf{C3}\cdot(\text{A})^2$) as is β -H elimination ($\Delta G^\ddagger = 19.0 \text{ kcal mol}^{-1}$ relative to $\mathbf{C3}\cdot(\text{A})^2$). It is the unfavourable thermodynamic profile of the nucleophilic attack, which favours $\mathbf{C3}\cdot\text{S}\cdot\text{A}$ somewhat over $\mathbf{C4}\cdot\text{A}$, that makes the second hydrogen transfer more demanding kinetically. As can be anticipated, the incoming pyrrolidine is likely to displace the silazane product P at $\mathbf{C5}\cdot\text{P}\cdot\text{A}$ readily.^[43] It renders the stepwise $\mathbf{C3}\cdot(\text{A})^2 \rightarrow \mathbf{C3}\cdot\text{S}\cdot\text{A} \rightarrow \mathbf{C4}\cdot\text{A} \rightarrow \mathbf{C5}\cdot\text{P}\cdot\text{A} \rightarrow \mathbf{C5}\cdot(\text{A})^2$ silazane formation almost thermoneutral, with the second hydrogen transfer to barium dictating the overall kinetics of this process.

On the other hand, despite all our efforts, a low-energy TS structure describing Ba–N/Si–H σ -bond-breaking metathesis, which would represent the concerted silazane-generating analogue (see Scheme 5), could not be located. The careful examination of the metathetical transformation with the aid of a reaction-path-optimisation (chain-of-states) method using suitably guessed initial TS structures resulted in minimum-energy pathways describing either nucleophilic attack or hydrogen transfer (depending on the initial TS guess) as energetically prevalent alternatives. This let us conclude with some confidence that higher kinetic demands would be associated with the alternative concerted pathway and is thus unlikely to have any relevance for barium catalyst turnover. As to whether these findings hold true for more compact alkaline earths will be analysed below.

The subsequent protonolysis of pyrrolidine by the $\{\text{N}^{\wedge}\text{N}\}\text{Ba}$ hydride converts $\mathbf{C5}$ back into the catalytically competent $\{\text{N}^{\wedge}\text{N}\}\text{Ba}$ pyrrolide for another catalyst turnover. The process to start from either mono- or bis-pyrrolidine adducted $\{\text{N}^{\wedge}\text{N}\}\text{Ba}$ hydride species evolves through a metathesis-type TS structure (see Figure S2 in the Supporting Information) that decays thereafter into amine-free and amine-adducted forms of the $\{\text{N}^{\wedge}\text{N}\}\text{Ba}$ pyrrolide compound through facile liberation of one equiv of H_2 . The participation of one adducted

amine spectator molecule facilitates the process greatly on thermodynamic and also kinetic grounds, thereby paralleling the findings for the preceding nucleophilic attack step, and causes moreover the direct expulsion of H₂ after TS[C5•(A)²–C3•A] is traversed. In light of a kinetically easy ($\Delta G^\ddagger = 9.6$ kcal mol⁻¹ relative to C5•(A)²) pyrrolidine C5•(A)²→C3•A + H₂ (+A)→C3•(A)² protonolysis that is furthermore almost thermoneutral (Figure 11), {N^N}Ba hydride C5•(A)² and {N^N}Ba pyrrolide C3•(A)² compounds can readily interconvert and are thus expected participating in a mobile equilibrium.

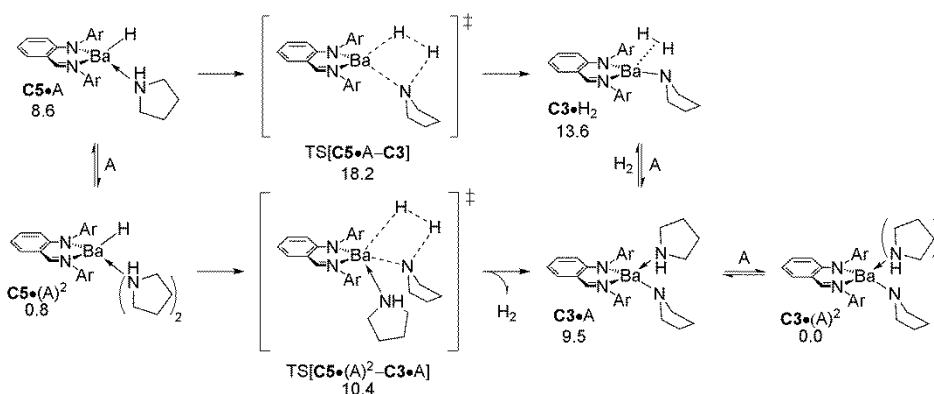
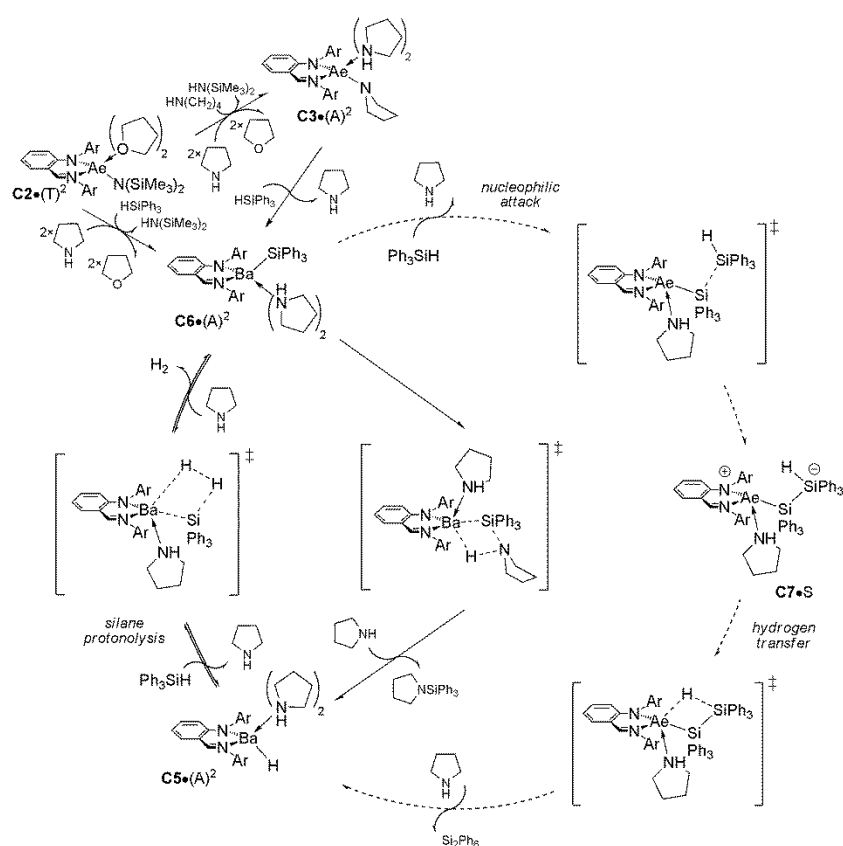


Figure 11. Protonolysis of the pyrrolidine by the {N^N}Ba hydride C5.^[43,44a]

B – Pathways commencing from the {N^N}Ba silyl

We now turn to the mechanistic branch that starts from {N^N}Ba silyl compound **C6** (Scheme 6). The Ba–N amido σ -bond silanolysis at {N^N}Ba pyrrolide **C3** has been studied as a plausible route that leads to the generation of **C6**. The process to start from the thermodynamically prevalent C3•(A)² sees the initial displacement of pyrrolidine by triphenylsilane, which leads to C3•S•A or, after the release of another adducted amine molecule, to C3•S encounter species and to proceed thereafter via a metathesis-type TS structure to furnish mono- or bis-amine adducts of **C6** (see Figure S3 in the Supporting Information). The exchange of the pyrrolide for the silyl group at C3•(S)² requires a barrier of

21.3 kcal mol⁻¹ to overcome along the most accessible pathway (Figure 12), which involves an additionally associated spectator amine molecule, but favours the {N[^]N}Ba pyrrolide ($\Delta G = 8.0$ kcal mol⁻¹). It characterises the $\mathbf{C3}\cdot(\mathbf{A})^2 + \mathbf{S} (-\mathbf{A}) \rightarrow \mathbf{C6}\cdot(\mathbf{A})^2$ generation of the {N[^]N}Ba silyl to be kinetically viable. Moreover, $\mathbf{C6}\cdot(\mathbf{A})^2$ (and $\mathbf{C6}\cdot\mathbf{A}$) precursor species for silazane formation are found somewhat more stable than encounter species $\mathbf{C3}\cdot\mathbf{S}\cdot\mathbf{A}$ (and $\mathbf{C3}\cdot\mathbf{S}$) that are involved along the alternative mechanistic branch for silazane formation and hence can be expected to be populated in similar, appreciable amounts.



Scheme 6. Plausible mechanistic pathways for iminoanilide alkaline-earth-catalysed CDC of amines and silanes, with [{N[^]N}Ae{Si(C₆H₅)₃}] (**C6**) as the catalytically competent compound and triphenylsilane (**S**) and pyrrolidine (**A**) substrates. A rival pathway for silane homocoupling is also shown. ({N[^]N}⁻ = [ArN(*o*-C₆H₄)C(H)=NAr]⁻ with Ar = 2,6-*i*Pr-C₆H₃).

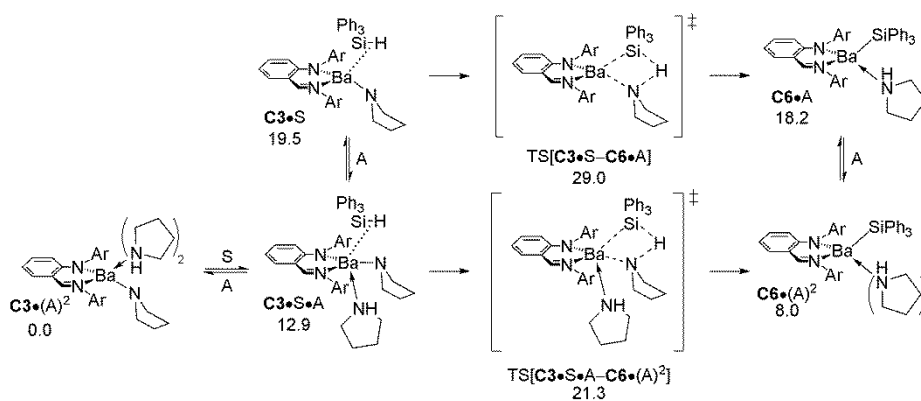


Figure 12. Ba–N pyrrolide σ -bond protonolysis at **C3** by silane substrate **S**.^[43,44a]

The generation of silazane product **P** to start from the $\{N^{\wedge}N\}$ Ba silyl **C6(A)ⁿ** preferably evolves through $TS[C6(A)^2-C5(P)A]$ describing concerted Ba–Si/N–H σ -bond breaking metathesis in the presence of an adducted pyrrolidine spectator molecule (see Figure S4 in the Supporting Information). Additional pyrrolidine readily displaces the silazane **P** from **C5(P)A** to yield **C5(A)²**,^[43] which renders the overall process (relative to **C3(A)²**) virtually thermoneutral. Despite its favourable thermodynamics the assessed prohibitively high barrier in excess of 64 kcal mol⁻¹ (Figure 13) characterises the Si–N/Ba–H σ -bond forming metathesis to be inaccessible kinetically. This result parallels the findings of a previous computational study on silane dehydrocoupling by some rare earth compounds.^[45]

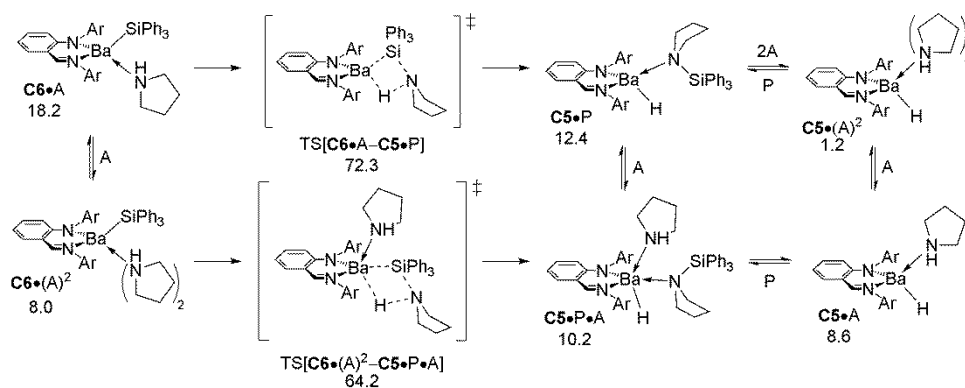


Figure 13. Ba–Si/N–H σ -bond breaking metathesis at $\{N^{\wedge}N\}$ Ba silyl compound **C6**.^[43,44a]

Moreover, the protonolysis of silane by the {N^N}Ba hydride (see Figure S5 in the Supporting Information) that would follow thereafter, thereby regenerating the {N^N}Ba silyl compound, is found to be more demanding energetically (Figure 14) when compared to the related protonolysis of pyrrolidine (Figure 11) via the alternative reaction branch. It is worth noting that the barrier associated to the prevalent $\text{C5}\cdot\text{S}\cdot\text{A}\rightarrow\text{C6}\cdot\text{A} + \text{H}_2 (+\text{A})\rightarrow\text{C6}\cdot(\text{A})^2$ pathway for silane protonolysis exceeds the overall barrier for silazane generation that starts at the {N^N}Ba pyrrolide complex.

Taking all these findings together, one can confidently dismiss the reaction branch that is initiated by the conversion of {N^N}Ba pyrrolide (or {N^N}Ba silylamide starting material $\text{C2}\cdot(\text{T})^2$) into the {N^N}Ba silyl and involves Ba–Si/N–H σ -bond breaking metathesis to be followed by silane protonolysis, in the presence of an energetically prevalent pathway for stepwise silazane formation (Figures 10, 11) with the {N^N}Ba pyrrolide as the catalytically competent compound. The turnover-limiting β -H elimination accounts for the rate acceleration observed for a silane with an electron-withdrawing group in *para* position, the negative charge build up at silicon (given that a transient silicate intermediate featuring a hypervalent silicon centre is involved) as indicated by a Hammett analysis of substituted silanes and also for the substantial primary kinetic isotope effect. Moreover, the Hammett analysis, which is inconsistent with other examples of σ -bond metathesis processes that have not shown substantial charge accumulation in the TS,^[46] provides further support for the operation of the pathway for stepwise silazane formation. The DFT-assessed activation energy for turnover-limiting β -H elimination satisfactorily matches empirically determined Eyring parameters.

These findings rationalise the distinct deviation in reactivity observed for strontium pyrrolide **9-Sr** and bis-silanide **5-Sr** (see Table 1). On the one hand, **9-Sr** does not require further transformation prior to passing through the most accessible pathway and is thus found

competent to mediate CDC catalysis. In contrast, an Ae silyl compound is seen to be incapable of effecting silazane formation and would thus make an initial conversion into an Ae amide indispensable for CDC catalysis to proceed. The **5-Sr** appears less effective in mediating such transformation and/or subsequent nucleophilic attack and β -H elimination steps, hence rendering **5-Sr** inactive catalytically.

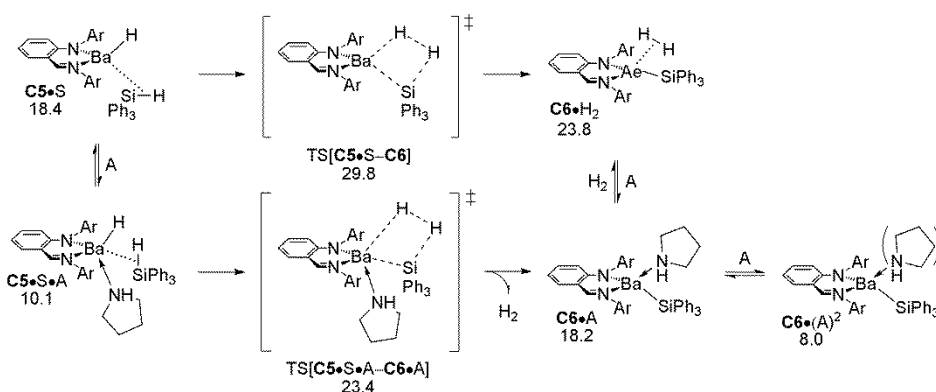


Figure 14. Protonolysis of the silane by the {N^N}Ba hydride **C5**.^[43,44a]

Although disilanes are not part of the observed product spectrum, we thought it would be informative to examine the rival homocoupling of triphenylsilane **S** in the presence of {N^N}Ba silyl **C6** (see Figure S6 in the Supporting Information). Both stepwise and concerted pathways are conceivable, but a stepwise pathway (shown dashed in Scheme 6), which bears formal similarity with the one shown in Figure 10, is found energetically prevalent. Alike to what has been discovered for all the steps studied thus far, one associated amine spectator molecule **A** greatly facilitates silane homocoupling. In light of their formal analogy, it is tempting to compare the inherent propensity of the {N^N}Ba silyl **C6** and {N^N}Ba pyrrolide **C3** to nucleophilically attack triphenylsilane **S** and to effect β -H elimination from a five-coordinate silicon centre onto the alkaline earth. Considering intrinsic barriers as a valuable means, Si–Si bond formation via **C6•S•A**→**C7•A** is seen to be more

demanding kinetically and also thermodynamically ($\Delta G_{\text{int}}^{\ddagger}/\Delta G_{\text{int}} = 13.8/9.9$ kcal mol⁻¹ relative to **C6•S•A**; Figure 15) when compared with **C3•S•A**→**C4•A** N–Si bond formation ($\Delta G_{\text{int}}^{\ddagger}/\Delta G_{\text{int}} = 4.5/1.3$ kcal mol⁻¹ relative to **C3•S•A**; Figure 10); this thereby reflects the enhanced nucleophilicity of the pyrrolide N centre together with some steric constraints associated with silane homocoupling. By contrast, β-H elimination from the hypervalent silicon centre at transient silicate intermediates **C7•A** ($\Delta G_{\text{int}}^{\ddagger} = 5.4$ kcal mol⁻¹ relative to **C7•A**; Figure 15) and **C4•A** ($\Delta G_{\text{int}}^{\ddagger} = 4.8$ kcal mol⁻¹ relative to **C4•A**; Figure 10) is equally found highly facile. Despite its associated low intrinsic barrier, the fact that the nucleophilic attack of the {N^N}Ba silyl is strongly uphill renders the second hydrogen transfer step to determine the overall kinetics for the generation of Si₂Ph₆ and {N^N}Ba hydride **C5**. Figure 15 reveals a prohibitively large overall barrier ($\Delta G^{\ddagger} = 36.2$ kcal mol⁻¹ relative to **C3•(A)²**) for the rival silane homocoupling, which remains unachievable due to its non-competitive kinetic demands when compared with the most accessible stepwise pathway for silazane formation (Figures 10 and 11).

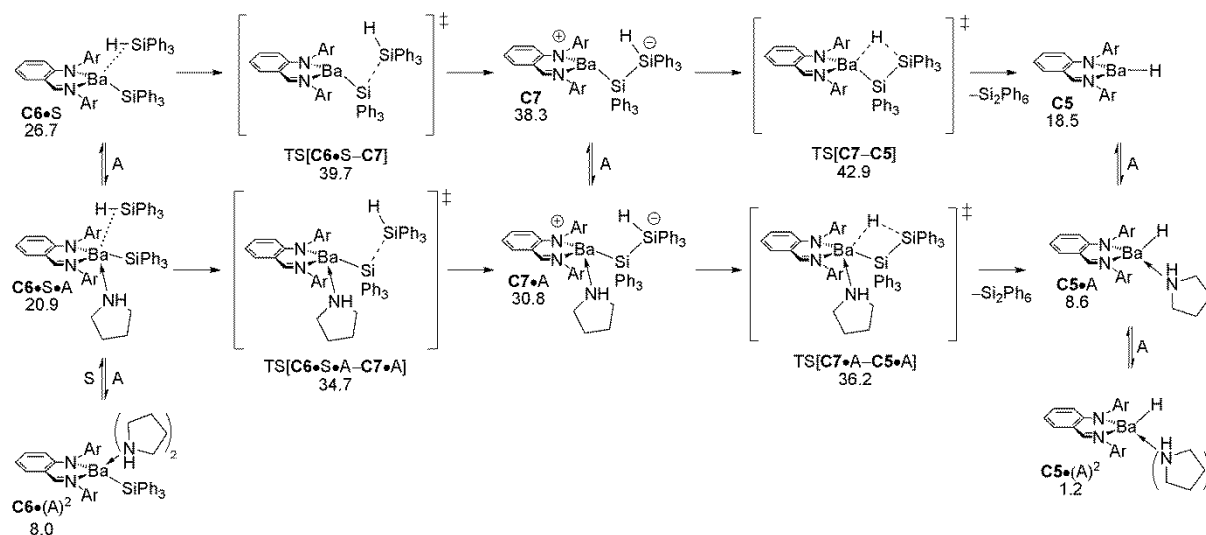


Figure 15. Nucleophilic attack of the {N^N}Ba silyl **C6** at the triphenylsilane **S** together with subsequent hydrogen transfer to barium at the transient intermediate **C7** to afford {N^N}Ba hydride **C5** and the disilane Si₂Ph₆ product.^[43,44a]

C – Comparison of {N^N}Ae(NR₂)-mediated CDC (Ae = Ca, Sr, Ba)

We start with the examination of the accessibility of the pathway for concerted silazane formation in Scheme 5 for the calcium catalyst analogue. In contrast to the findings for barium, TS structures for Ae–N/Si–H σ -bond breaking metathesis could be located for the more compact calcium centre; key structural and energy features are summarised in Figures S7 and S8 (see the Supporting Information). Irrespective as to whether a spectator pyrrolidine molecule participates in metathesis pathways, they are found to be distinctly disfavoured kinetically ($\Delta\Delta G^\ddagger > 14$ kcal mol⁻¹, Figure S8) relative to the corresponding pathway for stepwise silazane production (Figure 16). The pronounced energy gap between stepwise and concerted pathways in Scheme 5 assessed for the calcium catalyst further corroborates our above conclusion that a σ -bond metathesis pathway remains inaccessible in the presence of an energetically prevalent stepwise pathway for all the studied alkaline earths.

Focusing now exclusively on the prevalent silazane-generating pathway shown in Figures 10 and 11, we now analyse to which extent the nature of the alkaline earth influences the relevant elementary steps. The generation of silazane P through consecutive nucleophilic attack and β -H elimination (Figure 16) and also the subsequent conversion of the {N^N}Ae hydride back into the catalytically competent {N^N}Ae pyrrolide (Figure 17) are seen to benefit from an adducted pyrrolidine spectator molecule involved. In light of the increase in the accessibility of the alkaline earth upon going down group 2, the regular growth of the thermodynamic gap between the **C3•(A)**² catalyst resting state and the **C3•S•A** precursor species for nucleophilic pyrrolide attack at S for ever more compact metal centres becomes understandable. The overall barrier associated with nucleophilic attack is likewise seen to increase regularly (Ca > Sr > Ba). Of particular note is the modest, but regular decrease of the intrinsic activation energy for ever heavier alkaline earths ($\Delta G_{\text{int}}^\ddagger = 5.3/4.7/4.5$ kcal mol⁻¹ for Ca/Sr/Ba, relative to **C3•S•A**) for the most accessible **C3•S•A**→**C4•A** pathway. Hence,

limitations in the accessibility of the Ae centre together with variations in the Ae–N pyrrolide bond strength contribute towards the greater energy demands for lighter alkaline earths, with the former factor clearly dominating. The subsequent β -H elimination appears to be turnover limiting for all the studied systems and its total barrier follows a regular Ca > Sr > Ba trend (Figure 16). It is perhaps instructive to have a closer look at the intrinsic process energetics ($\Delta G_{\text{int}}^{\ddagger} = 7.4/6.5/6.1$ kcal mol⁻¹ and $\Delta G_{\text{int}} = 3.0/-0.9/-2.7$ kcal mol⁻¹ for Ca/Sr/Ba, relative to **C3•S•A**). It displays again a regular trend, indicating that Ae–H bond formation becomes more favourable upon going down group 2 on both kinetic and thermodynamic grounds. Hence, a sterically less restricted barium centre in combination with an increased aptitude for Ae–H bond formation give rise to the enhanced performance of the barium catalyst when compared to its lighter analogues.

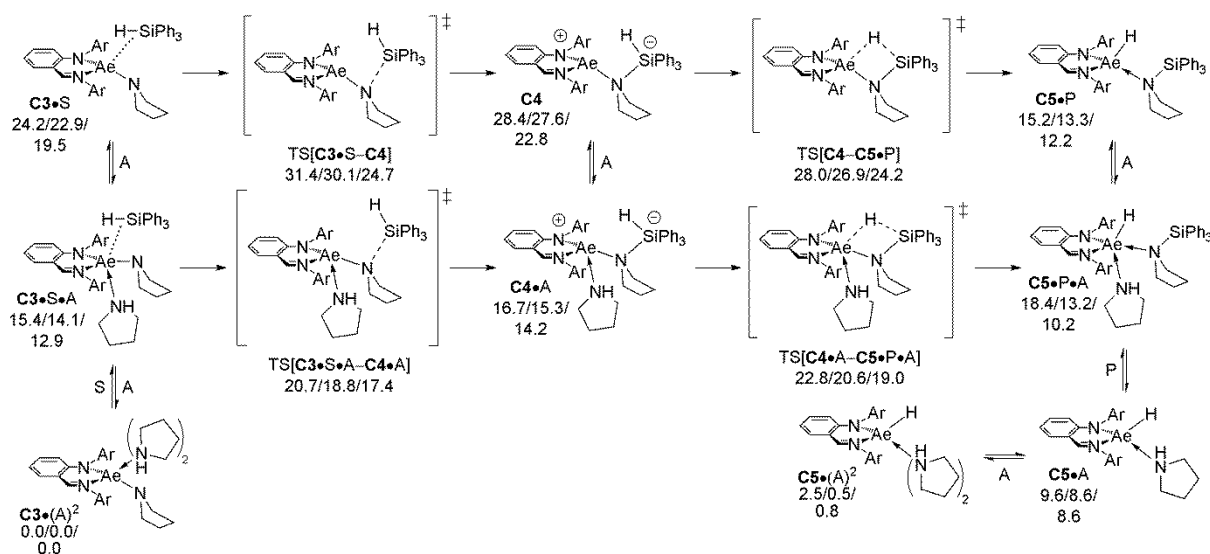


Figure 16. Nucleophilic attack of the {N^N}Ae pyrrolide **C3** at the triphenylsilane **S** together with subsequent hydrogen transfer to the alkaline earth at the transient silicate intermediate **C4** to afford {N^N}Ae hydride **C5** and the silazane (P) product (Ae = Ca/Sr/Ba).^[43,44]

The regeneration of the catalytically competent {N^N}Ae pyrrolide through protonolysis of pyrrolidine **A** by the {N^N}Ae hydride **C5** with the release of H₂ (Figure 17)

is found significantly less demanding kinetically than stepwise silazane formation (Figure 16) for the studied family of iminoanilide alkaline-earth catalysts. Given that the thermodynamic force that drives this conversion is rather small, $\{N^{\wedge}N\}Ae$ pyrrolide and hydride compounds can be expected to participate in a mobile equilibrium.

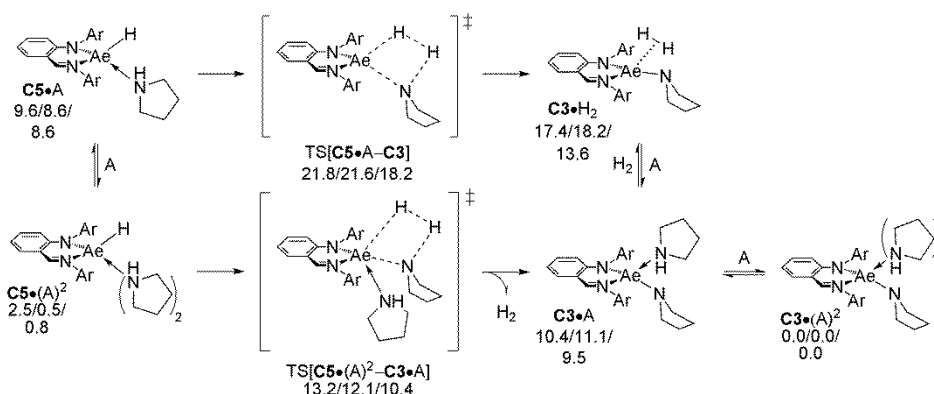


Figure 17. Protonolysis of pyrrolidine by the $\{N^{\wedge}N\}Ae$ hydride **C5** (Ae = Ca/Sr/Ba).^[43,44]

Summary and concluding remarks

Alkaline-earth metal complexes constitute excellent, chemoselective and versatile precatalysts for the production for a range of silazanes by cross-dehydrocoupling of amines and silanes. The scope of the reaction is large, and also includes di(amine)s and di(hydrosilane)s. Characteristically, the catalytic activity increases substantially upon going down in group 2, according to (Mg \ll) Ca < Sr < Ba. This observation has been rationalised by DFT computations, showing that greater accessibility of the metal centre and, to a lesser extent, increasing Ae–N_{amide} bond strength upon going to ever heavier alkaline earths, are behind this trend. However, these conclusions solely apply to the CDC catalysis presented herein, and should not be extended *a priori* to all Ae-mediated catalytic processes. The barium precatalysts $Ba[CH(SiMe_3)_2]_2 \cdot (THF)_3$ and $Ba[N(SiMe_3)_2]_2 \cdot (THF)_2$ display impressive

performance, and since their synthesis is relatively facile, they are to be recommended when the catalysed formation of silazanes is sought.

The operative mechanism of the Ae-mediated CDC catalysis has been established with a high level of confidence following a kinetic analysis and DFT investigations which considered several rival pathways. The computations show that in the presence of a catalytically competent iminoanilide barium amide or barium alkyl complex, pathways which involve a barium silyl to mediate CDC catalysis or to furnish a disilane by-product are non-competitive. This is fully consistent with the experimental data, as indeed the formation of these species was never detected spectroscopically during the monitoring of catalysed CDC reactions. Instead, complementary experimental and computational data provide conclusive evidence that the CDC of amines and organosilanes follows a stepwise reaction path consisting of (i) N–Si bond forming nucleophilic attack of the barium-pyrrolide onto the silane, followed (ii) by turnover-limiting β -hydrogen transfer to the Ba centre. A related mechanism was proposed for the $\{To^M\}Mg(N(SiMe_3)_2)$ CDC precatalyst, where nucleophilic attack has been proposed to be rate determining.^[20a]

That these Ae precatalysts are chemoselective and compatible with (dihydro)silanes, di(amine)s and di(hydrosilane)s opens up a range of synthetic possibilities. The synthesis of original poly(carbosilazane)s by coupling of di(amine)s and di(hydrosilane)s is an area where these Ae-mediated CDC processes can prove invaluable.^[32] Moreover, starting from an initial monohydrosilane (*e.g.* Ph_3SiH , Et_3SiH), stoichiometric cascade couplings of di(amine)s ($H_2NCH_2-C_6H_4-CH_2NH_2$, piperazine etc.) or primary amines (*e.g.* $BnNH_2$) with dihydrosilanes (*e.g.* Ph_2SiH_2) can yield unusual polysilazanes. Encoded and/or functionalised (macro)molecules can be prepared from judiciously selected bifunctional substrates such as arylsilanes with functional *p*-substituents. The Ae-promoted dehydrocoupling of amines with

boranes and the coupling of silanes with phosphines are other natural extensions of this work. Our efforts in these aims will be detailed in forthcoming reports.

Experimental section

General considerations. All manipulations were performed under inert atmosphere using standard Schlenk techniques or in a dry, solvent-free glove-box (Jacomex; O₂ < 1 ppm, H₂O < 5 ppm). AlMe₃ (2.0 M in toluene, Aldrich) was used as purchased. THF was distilled under argon from Na/benzophenone prior to use. Other solvents (pentane, toluene, dichloromethane, Et₂O) were collected from MBraun SPS-800 purification alumina columns. Deuterated solvents (Eurisotop, Saclay, France) were stored in sealed ampoules over activated 3 Å molecular sieves and degassed by several freeze-thaw cycles. Ae[N(SiMe₃)₂]₂•(THF)₂,^[47] Ae[N(SiMe₃)₂]₂,^[47a] Ae[N(SiMe₂H)₂]₂,^[25,48] Ae(CH₂SiMe₃)₂•(THF)₃,^[49] {N[^]N}Ae{N(SiMe₃)₂•(THF)_x}^[20c,25] and {N[^]N}Ae{CH(SiMe₃)₂•(THF)_x}^[20c,25] (Ae = Ca, Sr, Ba) were prepared following literature procedures.

NMR spectra were recorded on Bruker AM-400 and AM-500 spectrometers. All chemical shifts were determined using residual signals of the deuterated solvents and were calibrated vs. SiMe₄ and are given in ppm. Assignment of the signals was carried out using 1D (¹H, ¹³C{¹H}) and 2D (COSY, HMBC, HMQC) NMR experiments.

HR-MS data were recorded on a Bruker MicrOTOF-Q II mass spectrometer with an APCI (Atmospheric Pressure Chemical Ionisation) source in positive mode and direct introduction (ASAP – Atmospheric Solids Analysis Probe) at 370 °C.

Combustion analyses on **5-Sr** (C₄₈H₅₄O₃Si₂Sr, 822.75 g·mol⁻¹), **5-Ba** (C₄₈H₅₄O₃Si₂Ba, 872.45 g·mol⁻¹), **7-Ba** (C₄₃H₆₉N₃O₂Si₂Ba, 853.54 g·mol⁻¹) and **9-Sr** (C₃₉H₅₆N₄Sr, 668.53 g·mol⁻¹) were performed by Stephen Boyer on a Carlo-Erba analyser at the London Metropolitan University. Despite repeated (>4) attempts on different batches of each of these

compounds (including for crystals of **7-Ba** which were also characterised by XRD), we were unable to obtain satisfactory and reproducible elemental analyses for these compounds. This can certainly be attributed to the extreme air- and moisture-sensitivity of the complexes, and likely also to the presence of substantial amounts of silicon in the samples leading to the formation of non-pyrolisable silicon carbides.

NMR and spectroscopic characterisation of all new silazanes (isolated after quenching as solid materials upon evaporation of the volatiles and repeated washings with pentane) is available in the Supporting Information.

Sr(SiPh₃)₂•(THF)₃ (5-Sr). SrI₂ (300 mg, 0.8 mmol) was suspended in THF (10 mL) and stirred at 60 °C until dissolution was ensured (*ca.* 60 min). KSiPh₃ (500 mg, 1.6 mmol) was dissolved in THF (10 mL) and added dropwise *via* cannula to the solution of SrI₂ at room temperature. The reaction mixture was stirred for 2.5 h and a white precipitate gradually appeared. The precipitate was removed by filtration and the solvent was pumped off under vacuum. Complex **5-Sr** was obtained as a yellow powder (230 mg, 32%) after washing with pentane (3×5 mL). ¹H NMR (benzene-*d*₆, 500.1 MHz, 298 K): δ 7.76 (m, 12H, *o*-C₆H₅), 7.47 (m, 12H, *m*-C₆H₅), 7.12 (m, 6H, *p*-C₆H₅), 3.24 (m, 12H, OCH₂CH₂), 1.24 (m, 12H, OCH₂CH₂) ppm. ¹³C{¹H} NMR (benzene-*d*₆, 125.8 MHz, 298 K): δ 136.9 (*o*-C₆H₅), 136.4 (*m*-C₆H₅), 129.9 (*p*-C₆H₅), 68.4 (OCH₂CH₂), 25.6 (OCH₂CH₂) ppm. ²⁹Si{¹H} NMR (benzene-*d*₆, 79.5 MHz, 298 K): δ -12.14 ppm.

Ba(SiPh₃)₂•(THF)₃ (5-Ba). BaI₂ (328 mg, 0.8 mmol) was suspended in THF (10 mL) and stirred at 60 °C until dissolution was ensured (*ca.* 60 min). KSiPh₃ (500 mg, 1.6 mmol) was dissolved in THF (10 mL) and added dropwise *via* cannula to the solution of BaI₂ at room temperature. The reaction mixture was stirred for 2.5 h and a white precipitate gradually

appeared. The precipitate was eliminated by filtration and the solvent was removed under vacuum. Complex **5-Ba** was obtained as an orange powder (600 mg, 86%) after washing with pentane (3×5 mL). ^1H NMR (benzene- d_6 , 500.1 MHz, 298 K): δ 7.68 (m, 12H, *o*-C₆H₅), 7.46 (m, 12H, *m*-C₆H₅), 6.96 (m, 6H, *p*-C₆H₅), 3.54 (m, 12H, OCH₂CH₂), 1.40 (m, 12H, OCH₂CH₂) ppm. $^{13}\text{C}\{^1\text{H}\}$ NMR (benzene- d_6 , 125.8 MHz, 298 K): δ 136.63 (*o*-C₆H₅), 130.4 (*m*-C₆H₅), 125.9 (*p*-C₆H₅), 68.3 (OCH₂CH₂), 25.7 (OCH₂CH₂) ppm. $^{29}\text{Si}\{^1\text{H}\}$ NMR (benzene- d_6 , 79.5 MHz, 298 K): δ -12.11 ppm.

{N^N}Ba{N(SiMe₂H)₂}(THF)₂ (7-Ba). Anhydrous BaI₂ beads (446 mg, 1.14 mmol) was suspended in THF (10 mL) and activated at 60 °C for 60 min. KN(SiMe₂H)₂ (373 mg, 2.18 mmol) and {N^N}H (480 mg, 1.09 mmol) were dissolved in THF (10 mL) and the solution was added dropwise *via* cannula to the solution of BaI₂ at room temperature. The reaction mixture was stirred for 2.5 h and a white precipitate gradually appeared. The precipitate was removed by filtration and the solvent was pumped off under vacuum. Complex **7-Ba** was extracted with pentane (3×5 mL) and isolated as orange crystals (521 mg, 56%) by crystallisation at -27 °C. Crystals suitable for X-ray diffraction studies were selected from this batch. ^1H NMR (benzene- d_6 , 500.1 MHz, 298 K): δ 8.04 (s, 1H, CH=N), 7.28 (d, $^3J_{\text{HH}} = 7.6$ Hz, 2H, arom-*H*), 7.19 (m, 1H, arom-*H*), 7.12 (m, 3H, arom-*H*), 7.00 (m, 1H, arom-*H*), 6.92 (td, $^3J_{\text{HH}} = 8.6$ Hz, $^4J_{\text{HH}} = 1.8$ Hz, 1H, arom-*H*), 6.28 (dd, $^3J_{\text{HH}} = 8.2$ Hz, 1H, arom-*H*), 6.22 (d, $^3J_{\text{HH}} = 8.7$ Hz, 1H, arom-*H*), 4.71 (br, $^1J_{\text{HSi}} = 160$ Hz, 2H, Si(CH₃)₂H), 3.36 (m, 10H, OCH₂CH₂ (8H) + CH(CH₃)₂ (2H)), 3.18 (q, $^3J_{\text{HH}} = 6.8$ Hz, 2H, CH(CH₃)₂), 1.31 (m, 20H, OCH₂CH₂ (8H) + CH(CH₃)₂ (12H)), 1.23 (d, $^3J_{\text{HH}} = 6.7$ Hz, 6H, CH(CH₃)₂), 1.17 (d, $^3J_{\text{HH}} = 6.7$ Hz, 6H, CH(CH₃)₂), 0.24 (br, 12H, Si(CH₃)₂H) ppm. $^{13}\text{C}\{^1\text{H}\}$ NMR (benzene- d_6 , 125.8 MHz, 298 K): δ 169.2 (CH=N), 158.0 (N=CH-*i*-C₆H₄), 149.5 (ArN-*i*-C₆H₃), 146.6 (CH=N-*i*-C₆H₃), 144.6 (N-*i*-C₆H₄), 140.8 (ArN-*o*-C₆H₃), 139.6 (N=CH-*o*-C₆H₄), 133.7 (N-*o*-C₆H₄),

125.7 (CH=N-*o*-C₆H₃), 125.3 (ArN-*m*-C₆H₃), 124.8 (CH=N-*m*-C₆H₃), 124.7 (N=CH-*m*-C₆H₄), 118.6 (CH=N-*i*-C₆H₃), 118.4 (ArN-*p*-C₆H₃), 110.5 (N=CH-*p*-C₆H₄), 68.9 (OCH₂CH₂), 29.2 (CH(CH₃)₂), 28.5 (CH(CH₃)₂), 26.4 (CH(CH₃)₂), 26.2 (CH(CH₃)₂), 25.7 (OCH₂CH₂), 25.4 (CH(CH₃)₂), 23.8 (CH(CH₃)₂), 5.1 (Si(CH₃)₂H) ppm. FTIR (Nujol in KBr plates): $\nu = 2964$ (s), 2887 (s), 2004 (s), 1984 (sh), 1601 (sh), 1579 (m), 1380 (s), 1377 (s), 1359 (w), 1338 (s), 1234 (s), 1151 (s), 1097 (s), 1037 (w), 1004 (m), 947 (s), 916 (s), 887 (w), 827 (m) cm⁻¹.

{N[^]N}Sr{N(CH₂)₄•(HN(CH₂)₄) (9-Sr). {N[^]N}Sr{CH(SiMe₃)₂}₂•(THF)₂ (250 mg, 0.29 mmol) was dissolved in pentane (10 mL). Pyrrolidine (69 μ L, 0.86 mmol) was diluted in pentane (5 mL) and the solution was added dropwise *via* cannula to the solution. The reaction mixture was stirred for 2.5 h at room temperature. At the end of the reaction the solution was stored at -27 °C and **9-Sr** was isolated as an orange solid upon precipitation from solution (102 mg, 51%). ¹H NMR (benzene-*d*₆, 500.1 MHz, 298 K): δ 8.07 (s, 1H, CH=N), 7.25 (m, 3H, arom-*H*), 7.08 (m, 3H, arom-*H*), 7.01 (m, 1H, arom-*H*), 6.79 (td, ³*J*_{HH} = 6.8 Hz, ⁴*J*_{HH} = 3.4 Hz, 1H, arom-*H*), 6.21 (m, 2H, arom-*H*), 3.23 (br, 2H, CH(CH₃)₂), 3.05 (br, 2H, CH(CH₃)₂), 2.49 (br, 8H, HNCH₂CH₂ (4H) + SrN CH₂CH₂ (4H)), 1.27 (br, 8H, HNCH₂CH₂ (4H) + SrN CH₂CH₂ (4H)), 1.23 (d, ³*J*_{HH} = 6.9 Hz, 6H, CH(CH₃)₂), 1.11 (m, 12H, CH(CH₃)₂), 1.06 (d, ³*J*_{HH} = 6.7 Hz, 6H, CH(CH₃)₂), 0.94 (br, 1H, HN(CH₂)₄). ¹³C{¹H} NMR (benzene-*d*₆, 125.8 MHz, 298 K): δ 172.58 (CH=N), 160.0 (N=CH-*i*-C₆H₄), 149.7 (ArN-*i*-C₆H₃), 143.8 (CH=N-*i*-C₆H₃), 140.7 (ArN-*o*-C₆H₃), 139.5 (CH=N-*o*-C₆H₃), 133.5 (N-*i*-C₆H₄), 126.4 (CH=N-*o*-C₆H₃), 124.7 (N=CH-*m*-C₆H₄), 124.4 (N=CH-*p*-C₆H₄), 119.6 (ArN-*p*-C₆H₃), 116.4 (N-*o*-C₆H₄), 111.7 (CH=N-*p*-C₆H₃), 49.2 (BaNCH₂CH₂), 34.5 (HNCH₂CH₂), 29.3 (BaNCH₂CH₂), 28.7 (CH(CH₃)₂), 26.5 (CH(CH₃)₂), 25.7 (HNCH₂CH₂), 24.6 (CH(CH₃)₂), 23.8 (CH(CH₃)₂), 22.0 (CH(CH₃)₂), 22.7 (CH(CH₃)₂).

NMR-scale Generation of $\{N^{\wedge}N\}Ba\{N(SiMe_3)_2\} \cdot (HN(CH_2)_4)_2$ (10-Ba**).** In a glove-box, $\{N^{\wedge}N\}Ba\{N(SiMe_3)_2\} \cdot (THF)_2$ (10 mg, 0.011 mmol) was loaded into an NMR tube. The NMR tube was stored in a Schlenk tube, and it was removed from the glove-box and connected to the Schlenk manifold. The subsequent manipulations were performed using standard Schlenk techniques. C_6D_6 (0.5 mL) and pyrrolidine (*ca.* 2.0 μ L, 0.022 mmol) were added to the NMR tube. The NMR tube was sealed and shaken vigorously, then put into an oil bath at 25 °C for 2 h. The reaction mixture was directly analysed by 1H NMR. 1H NMR (benzene- d_6 , 500.1 MHz, 298 K): δ 8.05 (s, 1H, $CH=N$), 7.19 (d, $^3J_{HH} = 7.6$ Hz, 2H, arom- H), 7.16 (m, 1H, arom- H), 7.11 (m, 4H, arom- H), 6.91 (td, $^3J_{HH} = 8.6$ Hz, $^4J_{HH} = 1.8$ Hz, 1H, arom- H), 6.29 (dd, $^3J_{HH} = 8.0$ Hz, 1H, arom- H), 6.22 (d, $^3J_{HH} = 8.8$ Hz, 1H, arom- H), 3.50 (br, 2H, $CH(CH_3)_2$), 3.27 (hp, $^3J_{HH} = 6.8$ Hz, 2H, $CH(CH_3)_2$), 2.41 (br, 8H, $HN(CH_2)_4$), 1.33 (d, $^3J_{HH} = 7.0$ Hz, 6H, $CH(CH_3)_2$), 1.27 (br, 20H, $HNCH_2CH_2$ (8H) + $CH(CH_3)_2$ (12H)), 1.23 (d, $^3J_{HH} = 6.7$ Hz, 6H, $CH(CH_3)_2$), 0.60 (br, 2H, $HN(CH_2)_4$), 0.21 (s, 18H, $Si(CH_3)_3$) ppm. $^{13}C\{^1H\}$ NMR (benzene- d_6 , 125.8 MHz, 298 K): δ 169.3 ($CH=N$), 158.0 ($N=CH-i-C_6H_4$), 149.8 ($ArN-i-C_6H_3$), 146.6 ($CH=N-i-C_6H_3$), 141.0 ($ArN-o-C_6H_3$), 139.6 ($CH=N-o-C_6H_3$), 133.9 ($N-i-C_6H_4$), 126.0 ($CH=N-o-C_6H_3$), 124.9 ($N=CH-m-C_6H_4$), 124.9 ($N=CH-p-C_6H_4$), 124.7 ($ArN-p-C_6H_3$), 118.6 ($N-o-C_6H_4$), 111.1 ($CH=N-p-C_6H_3$), 50.3 ($HNCH_2CH_2$), 30.5 ($CH(CH_3)_2$), 29.4 ($CH(CH_3)_2$), 28.8 ($HNCH_2CH_2$), 26.4 ($CH(CH_3)_2$), 26.2 ($CH(CH_3)_2$), 25.7 ($CH(CH_3)_2$), 24.0 ($CH(CH_3)_2$), 5.8 ($Si(CH_3)_3$) ppm.

Typical procedure for catalysed CDC reactions. Catalysed cross-dehydrocoupling (CDC) reactions were carried out using the following standard protocol. In the glove-box, the precatalyst chosen from the families of compounds **1–9** (0.005 mmol, 1 equiv) was loaded into an NMR tube. The NMR tube was stored in an appropriate Schlenk tube, which was then removed from the glove-box to allow manipulations on a double manifold Schlenk line. The

subsequent manipulations were performed using standard Schlenk techniques. The amine ($n \times 0.005$ mmol, n equiv) and silane ($n \times 0.005$ mmol, n equiv) were syringed in the NMR tube. The NMR tube was sealed, removed from the Schlenk tube, shaken vigorously, and then placed in an oil bath at the desired temperature (298 or 333 K). After the required time period, the reaction was quenched as “wet” C_6D_6 was added to the mixture at room temperature. Substrate conversion was determined from the 1H NMR spectrum of the reaction mixture, comparing integrations characteristic of the substrates and products.

Procedure for kinetic measurements. The typical following protocol was used for catalysed CDC reactions monitored by 1H NMR spectroscopy: In a glove-box, pre-catalyst **6-Ba** and $HSiPh_3$ were loaded into an NMR tube. The NMR tube was stored in an appropriate Schlenk tube, which was then removed from the glove-box to allow manipulations on a double manifold Schlenk line. Using Schlenk techniques, pyrrolidine and C_6D_6 (0.5 mL) were then syringed in the NMR tube. The tube was sealed, removed from the Schlenk tube, vigorously shaken, and inserted into the probe of a Bruker AM 500 NMR spectrometer preheated at the required temperature. The reaction kinetics were monitored starting from this point using the *multi_zgvd* command of the TopSpin package ($D1 = 0.2s$; $DS = 0$; $NS = 8$ or more). Conversion was determined on the basis of amine consumption over the course of three or more half-lives, by comparing the relative intensities of resonances characteristic of the substrates and products.

X-ray diffraction crystallography. Crystals of **7-Ba** suitable for X-ray diffraction analysis were obtained by recrystallisation in pentane at -27 °C. Diffraction data were collected at 150(2) K using a Bruker APEX CCD diffractometer with graphite-monochromated $MoK\alpha$ radiation ($\lambda = 0.71073$ Å). A combination of ω and Φ scans was carried out to obtain at least

a unique data set. The crystal structures were solved by direct methods, remaining atoms were located from difference Fourier synthesis followed by full-matrix least-squares refinement based on F2 (programs SIR97 and SHELXL-97).^[50] Carbon- and oxygen-bound hydrogen atoms were placed at calculated positions and forced to ride on the attached atom. All non-hydrogen atoms were refined with anisotropic displacement parameters. The locations of the largest peaks in the final difference Fourier map calculation as well as the magnitude of the residual electron densities were of no chemical significance. Relevant collection and refinement data are given in the Supporting information. Crystal data, details of data collection and structure refinement for **7-Ba** (CCDC 1426816) are available from the Cambridge Crystallographic Data Centre via www.ccdc.cam.ac.uk/data_request/cif.

Computational Methodology. All calculations based on Kohn-Sham density functional theory (DFT)^[51] were performed by means of the program package TURBOMOLE^[52] employing flexible basis sets of triple- ζ quality. The Becke-Perdew (BP86)^[53] generalised gradient approximation (GGA) functional within the RI-*J* integral approximation^[54] in conjunction with appropriate auxiliary basis sets was used for structure optimisation. Empirical dispersion corrections by Grimme (D3 with Becke-Johnson damping)^[55] were used to account for non-covalent interactions. For alkaline-earth metals, we used the Stuttgart–Dresden scalar-relativistic effective core potential (SDD, 46 and 28 core electrons for Ba and Sr, respectively)^[56] in combination with the (7s7p5d1f)/[6s4p3d1f] (def2-TZVPP) valence basis set,^[57] whereas calcium was treated by the (17s12p4d)/[6s5p3d] (def2-TZVPP) all-electron basis set.^[57] All remaining elements were represented by Ahlrich’s valence triple- ζ TZVP basis set^[58a,b] with polarisation functions on all atoms. Final potential energies were obtained by single point-calculations at BP86-D3 optimised structures using the B97-D^[59] GGA functional (together with D3(BJ) empirical dispersion correction)^[55] in conjunction with

the aforementioned ECP/basis set for alkaline earths and a def2-TZVP^[54] basis set for all remaining elements (B97-D3/(SDD + def2-TZVP)//BP86-D3/(SDD + TZVP)). A large integration grid (*m4* in TURBOMOLE notation) and tight SCF convergence criteria have been used. The validity of the computational protocol employed for reliably mapping the energy landscape of alkaline-earth-mediated hydroamination has been substituted before^[39, 41g] and this allowed mechanistic conclusions with substantial predictive value to be drawn.

The reaction pathways were explored by a chain-of-states method^[60] as implemented in the module *woelfling* in the TURBOMOLE suite of programs, which makes use of reasonably chosen reactant and product structures to deliver an approximate to the minimum energy path (MEP). It identified the reactant and product states to be linked to the associated transition state. The approximate saddle points connected with the MEP were subjected to an exact localisation of the TS structures. No structural simplification of any of the key species involved was imposed nor have symmetry constraints have been imposed in any case. The DFT calculations simulated the authentic reaction conditions by treating the bulk effects of the benzene solvent by a consistent continuum model in form of the conductor-like screening model for realistic solvents (COSMO-RS)^[61] as implemented in *COSMOtherm*.^[62] This solvation model includes continuum electrostatic and also solvent-cavitation and solute-solvent dispersion effects through surface-proportional terms and also refers properly to a 1 M standard state. The free solvation enthalpy was assessed with the aid of COSMO-RS at the BP86/(SDD + def2-TZVPD)//BP86-D3/(SDD + TZVP) level of approximation. Geometry optimisation and frequency calculations were also performed at the BP86-D3/(SDD + SV(P))^[58c] level to confirm the nature of all optimised key structures and to determine thermodynamic parameters (298 K, 1 atm) under the conventional ideal-gas, rigid-rotor and quantum-mechanical harmonic-oscillator approximation. This level of basis-set quality is known to be reliable for the assessment of structural parameter and vibrational frequencies,^[63]

thus it allows an affordable and accurate determination of thermodynamic state functions. As far as the vibrational partition function is concerned, all frequencies below 60 cm^{-1} were replaced by a value of 60 cm^{-1} to correct for the quantum-mechanical harmonic-oscillator approximation for such normal modes (the quasi-harmonic approximation),^[64] and thermochemical contributions to enthalpy and entropy were computed from the resulting partition function. The entropy contributions for condensed-phase conditions were estimated based on computed gas-phase entropies (without any scaling applied) by employing the procedure of Okuno.^[65] The mechanistic conclusions drawn in this study were based on the Gibbs free-energy profile of the catalytic cycle assessed at the B97-D3(COSMO-RS)/(SDD + def2-TZVP) level of approximation for experimental condensed phase conditions. Calculated structures were visualised by employing the StrukEd program,^[66] which was also used for the preparation of 3D molecule drawings.

Supporting Information: Structural characterisation of DFT optimised key species involved in the various examined pathways; crystallographic data (including CIF file) for **7-Ba**; NMR and MS characterisation of all new silazanes; NMR for new complexes.

Acknowledgements: This work was sponsored by the French Ministry for Higher Education and Research (Ph. D. grant to C.B.).

References

- [1] a) J. F. Harrod, *Coord. Chem. Rev.* **2000**, 206–207, 493; b) R. Waterman, *Chem. Soc. Rev.* **2013**, 42, 5629; c) E. M. Leitao, T. Jurca, I. Manners, *Nature Chem.* **2013**, 5, 817; d) R. L. Melen, *Chem. Soc. Rev.*, DOI: 10.1039/c5cs00521c.
- [2] a) T. Wideman, L. G. Sneddon, *Chem. Mater.* **1996**, 8, 3; b) J. E. Mark, H. R. Allcock, R. West, *Inorganic Polymers 2nd ed.*, Oxford University Press, **2005**; c) T. Baumgartner, R. Réau, *Chem. Rev.* **2006**, 106, 4681; d) A. Nunns, J. Gwyther, I. Manners, *Polymer* **2013**, 54, 1269; e) A. K. Franz, S. O. Wilson, *J. Med. Chem.* **2013**, 56, 388.
- [3] M. Lappert, P. P. Power, A. Protchenko, A. Seeber, *Metal Amide Chemistry*, John Wiley & Sons, Ltd., Chichester, **2009**.
- [4] L. F. Fieser, M. Fieser, *Reagents in Organic Chemistry*, Wiley, New York, **1967**.
- [5] a) Y. Tanabe, M. Murakami, K. Kitaichi, Y. Yoshida, *Tetrahedron Lett.* **1994**, 35, 8409; b) Y. Tanabe, T. Misaki, M. Kurihara, A. Iida, Y. Nishii, *Chem. Commun.* **2002**, 1628.
- [6] a) P. J. Kocięński, *Protecting Groups, 3rd ed.*, Thieme, Stuttgart, **2005**, pp. 595-599; b) D. W. Robbins, T. A. Boebel, J. F. Hartwig, *J. Am. Chem. Soc.* **2010**, 132, 4068; c) S. Itagaki, K. Kamata, K. Yamaguchi, N. Mizuno, *Chem. Commun.* **2012**, 48, 9269; d) T. Tsuchimoto, Y. Iketani, M. Sekine, *Chem. Eur. J.* **2012**, 18, 9500; e) C. D. F. Königs, M. F. Müller, N. Aiguabella, H. F. T. Klare, M. Oestreich, *Chem. Commun.* **2013**, 49, 1506; f) L. Greb, S. Tamke, J. Paradies, *Chem. Commun.* **2014**, 50, 2318.
- [7] a) D. Seyferth, G. H. Wiseman, C. Prud'homme, *J. Am. Ceram. Soc.* **1983**, 66, C-13; b) D. Seyferth, G. H. Wiseman, *J. Am. Ceram. Soc.* **1984**, 67, C-132; c) Y. D. Blum, K. B. Schwartz, R. M. Laine, *J. Mater. Sci.* **1989**, 24, 1707; d) D. Seyferth, J. M. Schwark, R. M. Stewart, *Organometallics* **1989**, 8, 1980; e) W.-D. Wang, R. Eisenberg, *Organometallics* **1991**, 10, 2222; f) E. Duguet, M. Schappacher, A. Soum, *Macromolecules* **1992**, 25, 4835; g) N. R. Dando, A. J. Perrotta, C. Strohmman, R. M. Stewart, D. Seyferth, *Chem. Mater.* **1993**, 5, 1624; h) M. Birot, J.-P. Pilot, J. Dunoguès, *Chem. Rev.* **1995**, 95, 1443; i) D. Su, Y. Li, F. Hou, X. Yan, *J. Am. Ceram. Soc.* **2014**, 97, 1311.
- [8] R. Fessenden, J. S. Fessenden, *Chem. Rev.* **1961**, 61, 361.
- [9] a) L. H. Sommer, J. D. Citron, *J. Org. Chem.* **1967**, 32, 2470; b) J. F. Blandez, I. Esteve-Adell, M. Alvaro, H. García, *Catal. Sci. Technol.* **2015**, 5, 2167.

-
- [10] a) Y. Blum, R. M. Laine, *Organometallics* **1986**, *5*, 2081; b) C. Biran, Y. D. Blum, R. Glaser, D. S. Tse, K. A. Youngdahl, R. M. Laine, *J. Mol. Catal.* **1988**, *48*, 183; c) C. K. Toh, H. T. Poh, C. S. Lim, W. Y. Fan, *J. Organomet. Chem.* **2012**, *717*, 9.
- [11] W. D. Wang, R. Eisenberg, *Organometallics* **1991**, *10*, 2222.
- [12] E. J. Matarasso-Tchiroukhine, *Chem. Soc., Chem. Commun.* **1990**, 681.
- [13] H. Q. Liu, J. F. Harrod, *Can. J. Chem.* **1992**, *70*, 107.
- [14] a) H. Q. Liu, J. F. Harrod, *Organometallics* **1992**, *11*, 822; b) for the related coupling of hydrosilanes and hydrazines, see: J. He, H. Q. Liu, J. F. Harrod, R. Hynes, *Organometallics* **1994**, *13*, 336.
- [15] L. K. Allen, R. García-Rodríguez, D. S. Wright, *Dalton Trans.* **2015**, *44*, 12112.
- [16] A. E. Nako, W. Chen, A. J. P. White, M. R. Crimmin, *Organometallics* **2015**, *34*, 4369.
- [17] a) K. Takaki, T. Kamata, Y. Miura, T. Shishido, K. Takehira, *J. Org. Chem.* **1999**, *64*, 3891; b) K. Takaki, K. Komeyama, K. Takehira, *Tetrahedron* **2003**, *59*, 10381; c) F. Buch, S. Harder, *Organometallics* **2007**, *26*, 5132; d) W. Xie, H. Hu, C. Cui, *Angew. Chem. Int. Ed.* **2012**, *51*, 11141.
- [18] J. X. Wang, A. K. Dash, J.-C. Berthet, M. Ephritikhine, M. S. Eisen, *J. Organomet. Chem.* **2000**, *49*, 610.
- [19] T. Tsuchimoto, Y. Iketani, M. Sekine, *Chem. Eur. J.* **2012**, *18*, 9500.
- [20] a) J. F. Dunne, S. R. Neal, J. Engelkemier, A. Ellern, A. D. Sadow, *J. Am. Chem. Soc.* **2011**, *133*, 16782; b) M. S. Hill, D. J. Liptrot, D. J. MacDougall, M. F. Mahon, T. P. Robinson, *Chem. Sci.* **2013**, *4*, 4212; c) C. Bellini, J.-F. Carpentier, S. Tobisch, Y. Sarazin, *Angew. Chem. Int. Ed.* **2015**, *54*, 7679.
- [21] The NMR data were unambiguous regarding the formulation and structure of **9-Sr**, which clearly contained one coordinated molecule of pyrrolidine. On the other hand, we could not clearly assess the exact formulation of its barium congener **9-Ba**: the ¹H NMR spectrum of the obtained complex suggested the presence of one to two molecules of pyrrolidine, and we were not able to remove the doubt on its actual composition. Elemental analyses were not informative, and we failed in our attempts to obtain X-ray quality crystals. See the Supporting Information (Figure S8) for detail.
- [22] R. J. P. Corriu, C. Guérin, *J. Chem. Soc., Chem. Commun.* **1980**, 168.
- [23] The pale yellow calcium derivative Ca(SiPh₃)₂•(THF)₄ ($\delta_{29\text{Si}} = -13.99$ ppm), where the metal is stabilised by four THF molecules instead of three as in **5-Sr** and **5-Ba**, was recently reported: a) V. Leich, T. P. Spaniol, L. Maron, J. Okuda, *Chem. Commun.*

-
- 2014, 50, 2311; b) V. Leich, T. P. Spaniol, J. Okuda, *Inorg. Chem.* **2015**, 54, 4927. The difference in the ^{29}Si chemical shifts between $\text{Ca}(\text{SiPh}_3)_2 \cdot (\text{THF})_4$ and **5-Sr/5-Ba** ($\delta_{29\text{Si}} = -12.14$ and -12.11 ppm) reflects the presence of one extra THF molecule in the calcium complex, and these values altogether hint at highly ionic $\text{Ae} \cdots \text{Si}$ bonding. For other examples of alkaline-earth silanides, see: c) W. Teng, U. Englich, K. Ruhlandt-Senge, *Angew. Chem. Int. Ed.* **2003**, 42, 3661; d) D. J. Liptrot, M. Arrowsmith, A. L. Colebatch, T. J. Hadlington, M. S. Hill, G. Kociok-Köhn, M. F. Mahon, *Angew. Chem. Int. Ed.* DOI:10.1002/anie.201507004.
- [24] Y. Sarazin, D. Roşca, V. Poirier, T. Roisnel, A. Silvestru, L. Maron, J.-F. Carpentier, *Organometallics* **2010**, 29, 6569.
- [25] B. Liu, T. Roisnel, J.-F. Carpentier, Y. Sarazin, *Chem. Eur. J.* **2013**, 19, 13445.
- [26] In a similar fashion, we have checked that the NMR-scale reaction (C_6D_6 , 298 K) of 2 equiv of pyrrolidine with the bis-alkyl complex **4-Ba** releases $\text{CH}_2(\text{SiMe}_3)_2$ quantitatively, whereas with the bis-amide **1-Ba** the evolution of free $\text{HN}(\text{SiMe}_3)_2$ cannot be detected spectroscopically. See the Supporting Information, Figures S9-S11, for detail.
- [27] B. Liu, T. Roisnel, J.-F. Carpentier, Y. Sarazin, *Chem. Eur. J.* **2013**, 19, 2784.
- [28] a) O. Michel, K. W. Törnroos, C. Maichle-Mössmer, R. Anwander, *Chem. Eur. J.* **2011**, 17, 4964; b) O. Michel, K. W. Törnroos, C. Maichle-Mössmer, R. Anwander, *Eur. J. Inorg. Chem.* **2012**, 44.
- [29] B. Liu, T. Roisnel, J.-F. Carpentier, Y. Sarazin, *Angew. Chem. Int. Ed.* **2012**, 51, 4943.
- [30] Under identical conditions, the magnesium complexes did not afford significant catalytic activity. For instance, $\{\text{Mg}[\text{N}(\text{SiMe}_3)_2]_2\}_2$ only afforded 2% conversion of the substrates after 15 h reaction at 298 K with $[\text{pyrrolidine}]_0 = 4.0$ M and $[\text{pyrrolidine}]_0/[\text{Ph}_3\text{SiH}]_0/[\text{Mg}]_0 = 400:400:1$.
- [31] Under identical conditions to those given in Table 14, entry 6, the bis-silazido barium complex **5-Ba** also proved totally inactive. On the other hand, the barium compound analogue to the pyrrolido complex **9-Sr** fully converted the substrates under the same conditions (*i.e.* those corresponding to Table 1, entry 8). However, due to the uncertainty as to the identity of this barium species (see ref. [21]), one should refrain from unduly data interpretation and must instead consider these results in the simplest qualitative manner.

-
- [32] Dehydropolymerisation reactions involving the catalysed coupling of di(amine)s and di(hydrosilane)s are specific applications which will be reported elsewhere: C. Bellini, J.-F. Carpentier and Y. Sarazin, *manuscript in preparation*.
- [33] For instance, under discriminating conditions ($[\text{diamine}]_0/[\text{silane}]_0/[\mathbf{1-Ba}]_0 = 20:40:1$, $[\text{diamine}]_0 = 0.2 \text{ M}$, 298 K, 2.5 h), substrate conversion in the coupling of *N,N'*-dimethylethylenediamine with triphenylsilane catalysed by **1-Ba** reached 43%, 45% and 40% in C_6D_6 , $\text{C}_6\text{D}_5\text{Cl}$ and $\text{C}_6\text{D}_6/1,2\text{-C}_6\text{H}_4\text{F}_2$, respectively.
- [34] This disappointing result subsequently led us to assess the feasibility of the dehydrocoupling between Bn_2NH and Ph_3SiH . Very low conversions to $\text{Bn}_2\text{N-SiPh}_3$ were recorded with **1-Ba** (3%) and with **4-Ba** (7%) after 12 h at 333 K, with $[\text{Bn}_2\text{NH}]_0/[\text{Ph}_3\text{SiH}]_0/[\text{Ba}]_0 = 20:20:1$ and $[\text{Bn}_2\text{NH}]_0 = 0.1 \text{ M}$ in C_6D_6 . We are unable to explain the very poor reactivity of these dibenzyl-substituted amines in CDC reactions other than by arguing that steric factors may be unfavourable: the formation of the $[\text{Ba}]\text{-NBn}_2$ species required for catalytic turnover (see DFT section) may be sterically prohibited in the case of these congested amines.
- [35] The maximal kinetic isotope effect was calculated according to equations (a) and (b):
- $$k_{\text{Si-D}} / k_{\text{Si-H}} = e^{-\lambda} \quad (a)$$
- $$\lambda = (h c \nu_{\text{Si-H}}) / (2 k_{\text{B}} T) \times \{1 - (\mu_{\text{SiH}} / \mu_{\text{SiD}})^{1/2}\} \quad (b)$$
- where h is the Planck constant, c is the speed of light, k_{B} is the Boltzmann constant, μ_{SiH} and μ_{SiD} are the relevant effective masses, and $\nu_{\text{Si-H}}$ is the wavenumber for the stretching vibration of the N-H bond in the FTIR spectrum of the amine recorded at the temperature T . See: P. Atkins, J. de Paula, *Physical Chemistry (7th edition)*, Oxford University Press, Chichester, **2002**, pp. 888-889. We measured $\nu_{\text{Si-H}} = 2117 \text{ cm}^{-1}$ at $T = 290.5 \text{ K}$, giving $k_{\text{N-D}}/k_{\text{N-H}} = 4.35$.
- [36] Arrhenius analysis for the same data set gave $E_{\text{a}} = 16.2(23) \text{ kcal mol}^{-1}$.
- [37] For the values of sigma, see: C.G. Swain, E.C. Lupton, *J. Am. Chem. Soc.* **1968**, *90*, 4328.
- [38] B. Liu, T. Roisnel, J.-P. Guégan, J.-F. Carpentier, Y. Sarazin, *Chem. Eur. J.* **2012**, *18*, 6289.
- [39] S. Tobisch, *Chem. Eur. J.* **2014**, *20*, 8988.
- [40] B. Liu, J.-F. Carpentier, Y. Sarazin, *Chem. Eur. J.* **2012**, *18*, 13259.
- [41] a) S. Datta, M. T. Gamer, P. W. Roesky, *Organometallics* **2008**, *27*, 1207; b) M. Arrowsmith, M. S. Hill, G. Kociok-Köhn, *Organometallics* **2009**, *28*, 1730; c) M.

-
- Arrowsmith, M. S. Hill, G. Kociok-Köhn, *Organometallics* **2011**, *30*, 1291; d) J. Jenter, R. Köppe, P.W. Roesky, *Organometallics* **2011**, *30*, 1404; e) M. Arrowsmith, M. R. Crimmin, A. G. M. Barrett, M. S. Hill, G. Kociok-Köhn, P. A. Procopiou, *Organometallics* **2011**, *30*, 1493; f) M. Arrowsmith, M.S. Hill, G. Kociok-Köhn, *Organometallics* **2014**, *33*, 206; g) S. Tobisch, *Chem. Eur. J.* **2015**, *21*, 6765.
- [42] C. Brinkmann, A. G. M. Barrett, M. S. Hill, P. A. Procopiou, S. Reid, *Organometallics* **2012**, *31*, 7287.
- [43] a) Substrate association and dissociation at the various intermediates is presumably facile and rapid equilibria are expected; b) Examination by a linear-transit approach gave no indication that such processes are associated with a significant enthalpy barrier.
- [44] a) The prevalent pyrrolidine bis-amine adduct $3 \cdot (A)^2$ of the catalytically competent $[N^{\wedge}N]Ba\{N(CH_2)_4\}$ pyrrolide complex (with the appropriate number of substrate, silazane product or THF molecules) was chosen as reference for the relative free energies (given in kcal mol⁻¹); b) Free energies are given for calcium/strontium/barium analogues of relevant key species.
- [45] a) L. Perrin, O. Eisenstein, L. Maron, *New J. Chem.* **2007**, *31*, 549; b) L. Perrin, L. Maron, O. Eisenstein, T. D. Tilley, *Organometallics* **2009**, *28*, 3767.
- [46] M. E. Thompson, S. M. Baxter, A. R. Bulls, B. J. Burger, M. C. Nolan, B. D. Santarsiero, W. E. Schaefer, J. E. Bercaw, *J. Am. Chem. Soc.* **1987**, *109*, 203.
- [47] a) M. Westerhausen, *Inorg. Chem.* **1991**, *30*, 96; b) J. M. Boncella, C. J. Coston, J. K. Cammack, *Polyhedron* **1991**, *10*, 769; c) Y. Sarazin, R. H. Howard, D. L. Hughes, S. M. Humphrey, M. Bochmann, *Dalton Trans.* **2006**, 340.
- [48] N. Romero, S.-C. Roşca, Y. Sarazin, J.-F. Carpentier, L. Vendier, S. Mallet-Ladeira, C. Dinoi, M. Etienne, *Chem. Eur. J.* **2015**, *21*, 4115.
- [49] M. R. Crimmin, A. G. M. Barrett, M. S. Hill, D. J. MacDougall, M. F. Mahon, P. A. Procopiou, *Chem. Eur. J.* **2008**, *14*, 11292.
- [50] a) G. M. Sheldrick, SHELXS-97, Program for the Determination of Crystal Structures; University of Goettingen: Germany, 1997; b) G. M. Sheldrick, SHELXL-97, Program for the Refinement of Crystal Structures; University of Göttingen, Germany, 1997.
- [51] R. G. Parr, W. Yang, *Density-Functional Theory of Atoms and Molecules*, Oxford University Press, Oxford, **1989**.
- [52] a) R. Ahlrichs, M. Bär, M. Häser, H. Horn, C. Kölmel, *Chem. Phys. Lett.* **1989**, *162*, 165; b) O. Treutler, R. Ahlrichs, *J. Chem. Phys.* **1995**, *102*, 346; c) R. Ahlrichs, F.

-
- Furche, C. Hättig, W. Klopper, M. Sierka, F. Weigend, TURBOMOLE, version 6.6, University of Karlsruhe, Karlsruhe, (Germany), **2014**, <http://www.turbomole.com>.
- [53] a) P. A. M. Dirac, *Proc. R. Soc. (London) A* **1929**, *123*, 714; b) J. C. Slater, *Phys. Rev.* **1951**, *81*, 385; c) S. Vosko, L. Wilk, M. Nusiar, *Can. J. Phys.* **1980**, *58*, 1200; d) A. D. Becke, *Phys. Rev. A* **1988**, *38*, 3096; e) J. P. Perdew, *Phys. Rev. B* **1986**, *33*, 8822.
- [54] a) O. Vahtras, J. Almlöf, M. W. Feyereisen, *Chem. Phys. Lett.* **1993**, *213*, 514; b) K. Eichkorn, O. Treutler, H. Öhm, M. Häser, R. Ahlrichs, *Chem. Phys. Lett.* **1995**, *242*, 652.
- [55] a) S. Grimme, J. Anthony, S. Ehrlich, H. Krieg, *J. Chem. Phys.* **2010**, *132*, 154104; b) S. Grimme, S. Ehrlich, L. Goerigk, *J. Comput. Chem.* **2011**, *32*, 1456; c) <http://toc.uni-muenster.de/DFTD3/getd3.html>.
- [56] D. Andrae, U. Häußermann, M. Dolg, H. Stoll, H. Preuß, *Theor. Chim. Acta* **1990**, *77*, 123.
- [57] a) F. Weigend, R. Ahlrichs, *Phys. Chem. Chem. Phys.* **2005**, *7*, 3297; b) F. Weigend, *Phys. Chem. Chem. Phys.* **2006**, *8*, 1057.
- [58] a) A. Schäfer, C. Huber, R. Ahlrichs, *J. Chem. Phys.* **1994**, *100*, 5829; b) K. Eichkorn, F. Weigend, O. Treutler, R. Ahlrichs, *Theor. Chem. Acc.* **1997**, *97*, 119; c) A. Schäfer, C. Huber, R. Ahlrichs, *J. Chem. Phys.* **1992**, *97*, 2571.
- [59] a) S. Grimme, *J. Comput. Chem.* **2006**, *27*, 1787; b) A. D. Becke, *J. Chem. Phys.* **1997**, *107*, 8554.
- [60] P. Plessow, *J. Chem. Theory Comp.* **2013**, *9*, 1305.
- [61] a) A. Klamt, G. Schüürmann, *J. Chem. Soc. Perkin Trans. 2* **1993**, 799; b) A. Klamt, *J. Phys. Chem.* **1995**, *99*, 2224; c) F. Eckert, A. Klamt, *AIChE J.* **2002**, *48*, 369; d) A. Klamt, F. Eckert, W. Arlt, *Annu. Rev. Chem. Biomol. Eng.* **2010**, *1*, 101; e) A. Klamt, *WIREs Comput. Mol. Sci.* **2011**, *1*, 609.
- [62] F. Eckert, A. Klamt, COSMOtherm, Version C3.0, Release 13.01; COSMOlogic GmbH & Co. KG, Leverkusen (Germany), **2012**.
- [63] W. Koch, M. C. Holthausen, *A Chemist's Guide to Density Functional Theory*, 2nd Ed., Wiley-VCH, Weinheim, **2001**.
- [64] a) J. A. Keith, R. J. Nielsen, J. Oxgaard, W. A. Goddard III, *J. Am. Chem. Soc.* **2007**, *129*, 12343; b) R. F. Ribeiro, A. V. Marenich, C. J. Cramer, D. G. Truhlar, *J. Phys. Chem. B* **2011**, *115*, 14556.
- [65] Y. Okuno, *Chem. Eur. J.* **1997**, *3*, 212.

[66] For further details, see <http://www.struked.de>.

Alkaline-earth catalysed N–H/H–Si cross-dehydrocoupling

